

# Disentangling peri-urban river hypoxia

Ovidio García-Oliva<sup>a,\*</sup>, Carsten Lemmen<sup>a</sup>, Xiangyu Li<sup>b</sup> and Kai Wirtz<sup>a</sup>

<sup>a</sup>*Helmholtz-Zentrum hereon, Max-Planck-Straße 1, Geesthacht, 21502, Germany*

<sup>b</sup>*Leibniz Institute for Baltic Sea Research Warnemünde, Seestrasse 15, Rostock, 18119, Germany*

## ARTICLE INFO

**Keywords:**  
Biochemical model  
Temperature sensitivity  
Water quality  
Hypoxia  
Phytoplankton viral infections

## ABSTRACT

Episodes of low dissolved oxygen concentration—hypoxia—threaten the functioning of and the services provided by aquatic ecosystems, particularly those of urban rivers. Here, we disentangle oxygen-related processes in the highly modified Elbe River flowing through the major German city of Hamburg, where low oxygen levels are frequently observed. We use a process-based biochemical model that describes particulate and dissolved organic matter, micro-algae, their pathogens, and the key reactions that produce or consume oxygen: photosynthesis, re-aeration, respiration, mineralization, and nitrification. The model analysis reveals pronounced spatial variability in the relative importance of these processes. Photosynthesis and respiration are more prominent upstream of the city, while mineralization, nitrification, and re-aeration prevail downstream. The city, characterized by rapid changes in bathymetry, marks a transitional area: pathogen-related micro-algal lysis may increase organic material, explaining the shift towards heterotrophic processes downstream. As the primary driver of seasonal changes, the model analysis reveals a differential temperature sensitivity of biochemical rates. These results may be extrapolated to other urban rivers, and also provide valuable information for estuarine water quality management.

## 1. Introduction

Dissolved oxygen is a key indicator of water quality and ecosystem health (European Commission, 2006). Low oxygen levels (hypoxia) harm aerobic organisms and can trigger undesirable processes like greenhouse gas production and the release of nutrients and toxins from sediments (Bastviken et al., 2011; Salk et al., 2016). Despite the dominance of high oxygenation in—mostly turbulent—rivers, increasing evidence shows a trend to low-oxygen conditions worldwide, but particularly in urban areas (Mallin et al., 2006; Zhi et al., 2023; Blaszcak et al., 2023; Ma et al., 2024). This deoxygenation threatens the social, ecological, and biogeochemical functioning of urban rivers, such as fisheries or carbon and nutrient retention (Casas-Ruiz et al., 2017; Krause et al., 2022; Lespez et al., 2025; Grzyb and Kulczyk, 2023).

The riverine oxygen budget is governed by biochemical processes acting as sources (e.g., photosynthesis) or sinks (e.g., organic matter mineralization, respiration, abiotic reactions) of oxygen (Yakushev et al., 2013; Holzwarth and Wirtz, 2018). Air-water oxygen exchange—re-aeration—functions as either a source or sink relative to the temperature-dependent water saturation level (Wanninkhof, 2014; Carter et al., 2021). The relative importance of these processes varies with biochemical rates, which are influenced by flow velocity, nutrient loads, light irradiation, and water temperature (Holzwarth and Wirtz, 2018; Fan et al., 2025). These variables exhibit pronounced seasonal and interannual

variability, altering the dominance of each process throughout the year. But also droughts and floods alter particulate matter loads, impacting water turbidity, light availability, nutrient concentrations, and organic matter concentration (Graham et al., 2024; Bernal et al., 2025), and thereby affecting photosynthesis rates. Water temperature is particularly critical, as warming trends correlate with observed deoxygenation (Blaszcak et al., 2023). Understanding the drivers of oxygen dynamics requires disentangling the controlling biochemical processes responding to seasonally or intermittently changing river conditions.

This study focuses on oxygen-related processes in the highly modified urban Elbe River around Hamburg (Fig. 1), an area frequently experiencing summer hypoxia and fish mortality (Schaffrin et al., 2021). The Elbe River has a long history of monitoring and modeling efforts (e.g., Carstens et al., 2004; Schöl et al., 2014; Pein et al., 2021, 2025), with particular attention given to oxygen deficits at the Hamburg port (Schroeder, 1997; Schöl et al., 2014; Hein et al., 2018; Fan et al., 2025). We here employ the biogeochemical model **OxyPOM** (**O**xigen and **P**articulate **O**rganic **M**atter) coupled to the two-dimensional, depth-resolving river-following hydrodynamical model to simulate oxygen dynamics in 2020–2022. Our primary goal is the quantification of the relative importance of biochemical processes driving oxygen dynamics in this urban river in space and time, with emphasis on the role of temperature sensitivities.

## 2. Methodology

### 2.1. OxyPOM model description

A one-dimensional (only horizontal) long-channel predecessor version of OxyPOM was initially implemented by Holzwarth and Wirtz (2018) in the context of the closed-source Unstructured Tidal Residual Model–Delft Water Quality (UnTRIM DELWAQ) system used by the German

 ovidio.garcia@hereon.de (O. García-Oliva);  
carsten.lemmen@hereon.de (C. Lemmen); xiangyu.li@io-warnemuende.de (X. Li); kai.wirtz@hereon.de (K. Wirtz)  
ORCID(s): 0000-0001-6060-2001 (O. García-Oliva);  
0000-0003-3483-6036 (C. Lemmen); 0000-0001-6377-049X (X. Li);  
0000-0002-6972-3878 (K. Wirtz)

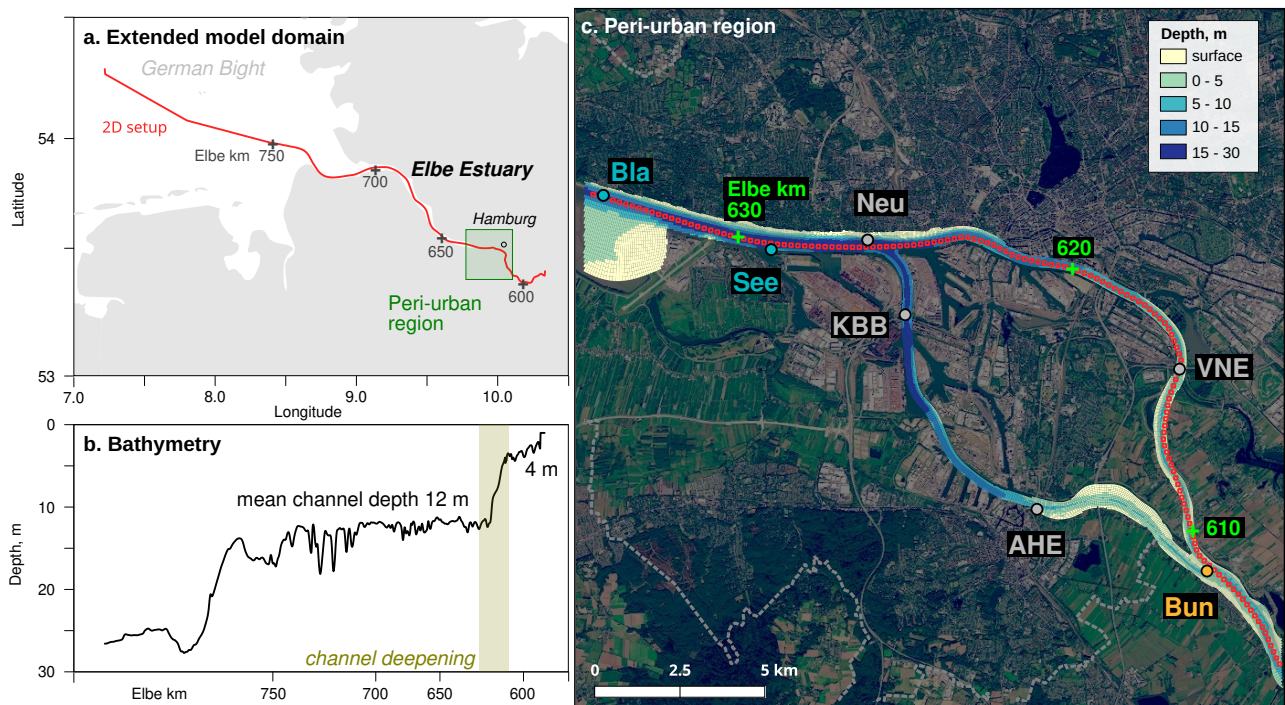


**Figure 1: Study area:** (a) The horizontal one-dimensional model domain ranges from Geesthacht weir (Elbe km 585) to the central German Bight. (b) The mean channel depth along this transect defines the bathymetry. (c) Focus on the peri-urban region with sampling stations. Upstream sampling stations (in light orange): Zol = Zollenspieker (not shown), and Bun = Bunthaus at Elbe km 599 and 609, respectively. Sampling stations in the city (in light gray): AHE = Alte Harburger Elbbrücke, KBB = Köhlbrandbrücke, VNE = Vogelsander Norderelbe, and Neu = Neumühlen at Elbe km 615, 614, 622 and 623, respectively. Downstream stations (in light blue): See = Seemannshöft, and Bla = Blankenese at Elbe km 629 and 634, respectively. Copernicus Sentinel data 2025.

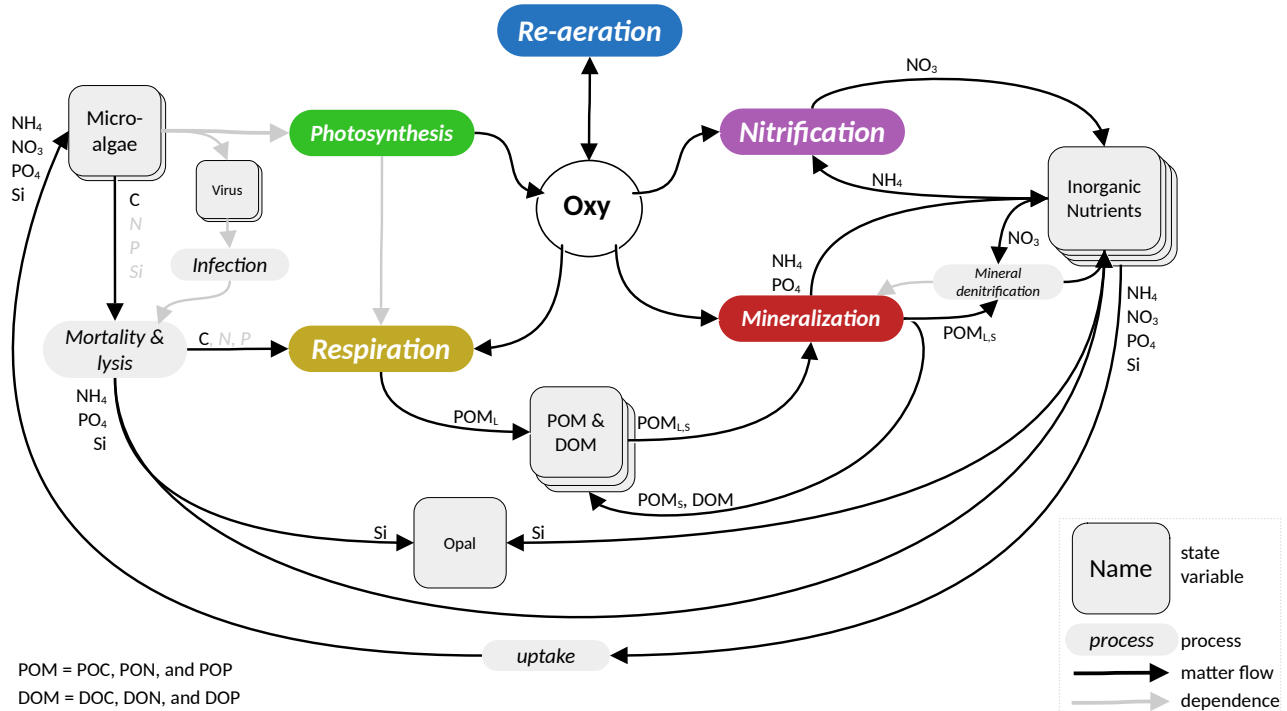


**Figure 2: Model configuration:** Processes consuming/producing dissolved oxygen (Oxy) resolved by OxyPOM. Other state variables and fluxes are also shown in a simplified way except for, e.g., settling and light attenuation. Grey symbols denote implicit fluxes defined by a fixed micro-algae stoichiometry.

Federal Waterways agency. This implementation lacked portability and did not adhere to FAIR principles (Findable, Accessible, Interoperable, Reusable Wilkinson et al., 2016). Our re-implementation as open source utilizes the Framework for Aquatic Biogeochemical Models Application Programming Interface (FABM API) (Bruggeman and Bolding, 2014), thereby ensuring accessibility, interoperability with other aquatic process models, and reusability across different hydrodynamic models and zero- to three-dimensional domains. Beyond the original implementation, we incorporated vertically-explicit formulations for re-aeration in rivers and estuaries (Raymond and Cole, 2001), primary production, and light attenuation; as new features, we included additional mortality terms for micro-algae, accounting for viral infections (Wirtz, 2019) and temperature-sensitive loss rates (Scharfe et al., 2009).

OxyPOM resolves the dynamics of dissolved oxygen (Oxy), labile and semi-labile particulate organic matter ( $POM_{L,S}$ ), silicate particles, dissolved organic matter (DOM), dissolved inorganic nutrients, two micro-algae classes, and two pathogenic viruses affecting micro-algae. POM and DOM are explicitly tracked for carbon, nitrogen, and phosphorus (C, N, P) content, with POM transitioning through labile and semi-labile states before dissolving. POM and DOM mineralization releases dissolved inorganic nitrogen, the sum of ammonium and nitrate, and ortho-phosphate; ammonium converts to nitrate depending on oxygen. Silicate is modeled in dissolved (bio-available) and particulate mineral (opal) forms. The model resolves two micro-algae classes, one also silicate-dependent representing diatoms. Their growth rates depend on the availability of light, dissolved nitrogen, and of ortho-phosphate. Micro-algal mortality, which is temperature-dependent and can also result from viral lysis, releases dissolved inorganic nutrients.

Dissolved oxygen dynamics is based on a mass balance equation:

$$\frac{dOxy}{dt} = \text{Re-aeration} + \text{Photosynthesis} - \text{Respiration} - \text{Nitrification} - \text{Mineralization.} \quad (1)$$

In Eq. 1, re-aeration (Eq. A.1) at the surface is a function of temperature, salinity, and wind speed (Weiss, 1970; Wanninkhof, 1992, 2014), with a correction for enhanced gas transfer at low wind speeds (Raymond and Cole, 2001). Photosynthesis (Eq. A.12) is limited by nutrient concentration and light intensity, following an exponential saturation relationship (Platt et al., 1980). Respiration (Eq. A.13) accounts for oxygen consumption by micro-algae. Oxygen is consumed by nitrification and mineralization (Eqs. A.26 and A.30, respectively) during ammonia oxidation and organic matter transformation, respectively. All these processes are expressed as temperature-sensitive biochemical rates using specific  $Q_{10}$  coefficients (Sherman et al., 2016). The full model description is included in the Supplementary material A.

## 2.2. Study area

We applied OxyPOM in the Elbe River using a two-dimensional vertically-resolved along-channel setup (Fig. 1). In the current application, we used the General Estuarine Transport Model (GETM) (Burchard and Bolding, 2002) as a hydrodynamic driver; GETM has demonstrated high skill for the Elbe estuary (Reese et al., 2024). The horizontal resolution is approximately 300 m, with a depth-adapting vertical resolution of 15 topography-following  $\sigma$ -layers—approximately 1 m at 15 m depth. The domain extends from the weir in Geesthacht (stream km 585) to the offshore area of the German Bight, and represents the mean channel depth rather than the maximum depth to maintain appropriate flow velocities (Schöl et al., 2014). Channel width was approximated by a simple power law formulation (Holzwarth and Wirtz, 2018). For this analysis, we focused on the freshwater zone of the river section across Hamburg (stream km 600–640), where low oxygen levels are frequently observed (Schöl et al., 2014).

## 2.3. Data sources

We reconstructed meteorological conditions, including air temperature, wind velocities, air pressure, total cloud cover, precipitation, and humidity, to an hourly resolution from eight stations operated by the German Weather Service (DWD, <https://opendata.dwd.de>). Boundary conditions on the ocean side were set to mean values for biogeochemical variables at Helgoland Roads (Wiltshire and Manly, 2004), with a sinusoidal water height emulating the tidal cycle and a seasonal changing temperature. On the river side, we reconstructed boundary conditions to a daily resolution from biogeochemical variables observed at the Geesthacht Weir by Wasser- und Schifffahrtsverwaltung (WSV, <https://www.kuestendaten.de>) and by Flussgebietsgemeinschaft (FGG) Elbe (<https://www.elbe-datenportal.de>), as well as water discharge at the Neu Darchau station from WSV.

For model validation, we used observations of biogeochemical variables—temperature, dissolved oxygen, chlorophyll, ortho-phosphate, nitrate, ammonia, particulate organic carbon (POC), and dissolved organic carbon (DOC)—from eight sampling stations in Hamburg: upstream (Zollenspieker and Bunthaus), in the city (Alte Harburger Elbbrücke, Köhlbrandbrücke, Vogelsander Norderelbe, and Neumühlen), and downstream (Seemannshöft and Blankenese); all data were sourced from WSV and FGG Elbe and downloaded from their official websites. Micro-algae biomass was calculated from chlorophyll concentration using as fixed conversion factor 0.05 g Chl-a g<sup>-1</sup> C (Holzwarth and Wirtz, 2018).

## 2.4. Performance metrics and model validation

Each model variable was evaluated at each observation station independently. We used  $N$  pairs of observed  $x^{\text{obs}}$  and modelled  $x^{\text{mod}}$  values, aggregated as daily means. We used four different performance metrics. The (i) coefficient of determination  $R^2$  for assessing whether the model captures the observational trend; (ii) the mean bias for assessing over- or underestimation:

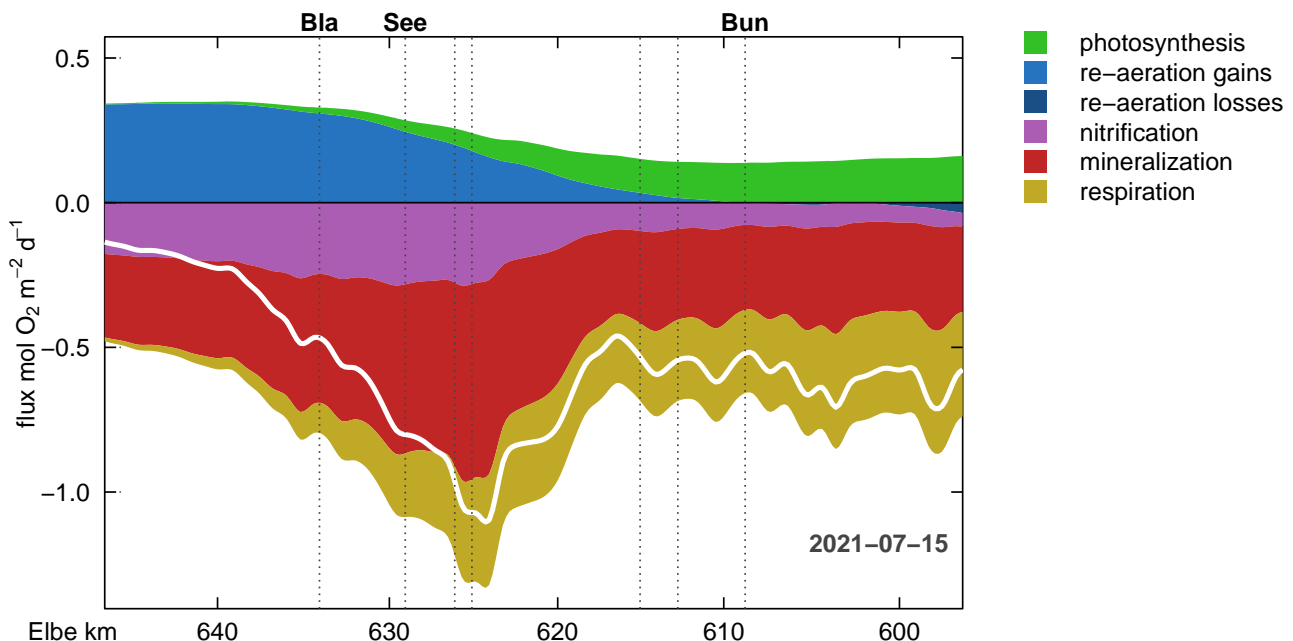


**Figure 3: Importance of re-aeration, photosynthesis, nitrification, mineralization and respiration in the oxygen flux (Eq. A.41, vertically integrated oxygen dynamics Eq. 1).** The dominant processes driving dissolved oxygen changes along the main channel during the most intense deoxygenation event July 15, 2021. The white line is the sum of all processes, showing a net deoxygenation rate. Bun = Bunthaus, See = Seemannshöft, Bla = Blankenese stations.

$$\text{bias} = \frac{1}{N} \sum_i (x_i^{\text{mod}} - x_i^{\text{obs}}); \quad (2)$$

(iii) the normalized square deviation (NSD)—is the model capturing the observed variability?

$$\text{NSD} = \frac{\text{SD}(x^{\text{mod}})}{\text{SD}(x^{\text{obs}})}, \quad (3)$$

where  $\text{SD}(x) = \sqrt{\frac{1}{N-1} \sum_i (x_i - \bar{x})^2}$  is the standard deviation with a mean  $\bar{x}$ ; and (iv) the hit rate (HR)—is the model representing the values within a limited range from the observations?

$$\text{HR} = \frac{1}{N} \sum_i n_i, \text{ with } n_i = \begin{cases} 1 & \text{if } |x_i^{\text{mod}} - x_i^{\text{obs}}| \leq D, \\ 0 & \text{otherwise} \end{cases}, \quad (4)$$

where  $D$  is the deviation, here defined as 20% of the range of observed values, thus  $D = 0.2 \cdot (\max(x_i^{\text{obs}}) - \min(x_i^{\text{obs}}))$ .

### 3. Results

#### 3.1. Spatial variability of oxygen sources and sinks

There is a notable degree of spatial variability in the dominance of various biochemical processes within the urban river ecosystem. These differences are stronger during

summer, when the oxygen minimum occurs (Fig. 3). Upstream of the city, photosynthesis and respiration dominate. The urban environment itself, marked by rapid fluctuations in bathymetry, functions as a transitional zone that alters the dynamics of these processes. Downstream areas exhibit a greater influence from mineralization, nitrification and re-aeration, indicating a shift in the dominant biochemical activities and physical processes as one moves through the urban landscape.

#### 3.2. Seasonal trends in the oxygen budget

The leading (de)oxygenation process varies by season (Fig. 4), notably through shifts in the role of re-aeration. In spring, as photosynthesis increases and becomes the main oxygen source, re-aeration is an oxygen sink, an effect that is more pronounced upstream than in the inner-city and downstream. Mineralization gains importance in summer and autumn, while respiration is the dominant oxygen sink from late winter into summer, with stronger impacts in the city and downstream. Nitrification strongly affects the oxygen budget upstream, depending on ammonia concentration, but its downstream contribution appears independent of local sources (see additional figure). In summer, photosynthesis remains dominant, re-aeration again becomes a source of oxygen, and higher oxygen demand from mineralization and respiration—driven by elevated organic material and faster micro-algae turnover—intensify deoxygenation; nitrification also contributes more prominently. In autumn, photosynthesis still supplies oxygen upstream but not in the city or downstream, and the roles of mineralization, respiration, and nitrification are similar to summer. In winter,

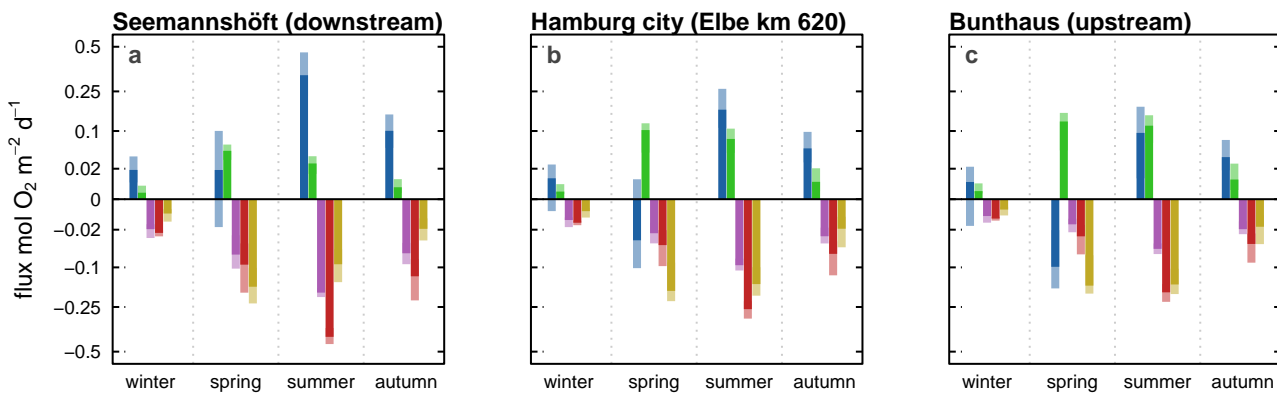


**Figure 4: Temporal variation in oxygen dynamics.** The absolute contribution of each process depends on the season as shown for three locations on the river: (a) downstream the city at Seemannshöft, (b) in the city (Elbe km 620), and (c) upstream of the city at Bunthaus. Legend as in Fig. 3, dark colors for the median value, lighter colors for the 25–75-percentile interval. Note the square-root-transformed y-axis.

photosynthesis is a source upstream but not downstream, and nitrification becomes the main deoxygenation process. This observation is consistent with the elevated ammonia discharge in late 2021 that was not observed in other years (see additional figure), alongside comparable respiration and reduced mineralization relative to autumn.

Overall, the net oxygen flux exhibits strong seasonal and along-river variability, with higher deoxygenation rates in summer and autumn ( $0.3\text{--}1.0 \text{ mol O}_2 \text{ m}^{-2} \text{ d}^{-1}$ ) and toward downstream locations (cf. Fig. 3f,g vs. 3e), and weaker deoxygenation in spring ( $0.3 \text{ mol O}_2 \text{ m}^{-2} \text{ d}^{-1}$ ) and near zero in winter.

### 3.3. Model performance

OxyPOM captures different responses for oxygen in stations upstream, in the city, and downstream (Fig. 5a). Larger differences among locations are observed in summer (for reference, red line in Fig. 5a is 15th of July, shown in Fig. 3). The model has good skill in reproducing oxygen when evaluated for each station independently, with  $1.0 < \text{NSD} < 1.3$  and  $0.85 < r^2 < 0.99$  for all stations (Fig. 5b). The aggregated evaluation shows good performance, with  $r^2 = 0.9$  ( $p < 2 \cdot 10^{-16}$ , 2678 degrees of freedom)—the model captures the observed trends, a mean bias of  $10.31 \text{ mmol m}^{-3}$ —the model overestimate dissolved oxygen, a normalized standard deviation of 1.09—the model reproduces the observed data variability, and a hit rate of 0.98 using a deviation of  $D$  of  $91 \text{ mmol m}^{-3}$ —the 98% of the modelled values lie within a  $\pm 91 \text{ mmol m}^{-3}$  from the observation (Fig. 5c). For a extended model validation see the Supplementary material B.

## 4. Discussion

Rivers are often seen as large reactors that process material before it is discharged into the sea (Casas-Ruiz et al., 2017). Our study demonstrates that the Elbe river is not one homogenous reactor but subdivided in time and

space in terms of dominant processes governing oxygen dynamics. Change points in oxygen dynamics are matched by those in other biogeochemical phenomena. Phytoplankton abundance, for example, quickly drops downstream of the city (Wiltshire and Schroeder, 1994; Martens et al., 2024a), along with changes in taxa composition (Martens et al., 2024b). These changes are translated to higher trophic levels, due to modifications in potential food quality and the trophic position of zooplankton (Biederick et al., 2025). The city is also a spatial boundary for marine bacteria (Branoff et al., 2024), silica release (Amann et al., 2014), nitrification and isotopic composition (Sanders et al., 2018), NO production (Ingeniero et al., 2024), and a transitional area for fauna composition (Schwentner et al., 2021). Downstream of the city—in the so-called “oxygen hole” (Tobias-Hünefeldt et al., 2024)—fish metabolites reveal respiration stress due to low oxygen conditions (Koll et al., 2024), and massive fish mortalities have been reported by news media, such as for 2021 (<https://www.wwf.de/2021/juni/grosses-sauerstoffloch-in-der-tideelbe-erste-hinweise-auf-fischsterben>). Moreover, the river’s function changes while crossing the city: Upstream, the river can be characterized as autotrophic due to higher photosynthesis rates with net oxygen production and carbon fixation; downstream, the river becomes heterotrophic due to higher mineralization rates with net oxygen consumption and carbon emission (Rewrie et al., 2025). A similar heterogeneity in leading (de)oxygenation processes has been observed in other urban rivers such as [here name some examples] (Huang et al., 2017; He et al., 2024).

As re-aeration depends on oxygen levels, its role may shift from a source to a sink depending on whether the water is saturated (Wanninkhof, 2014). As a surface process, re-aeration requires complete mixing of the water column to be effective as an oxygen source; otherwise, it primarily occurs in shallow waters, leaving deeper areas with low oxygen. Consequently, alterations in vertical mixing and

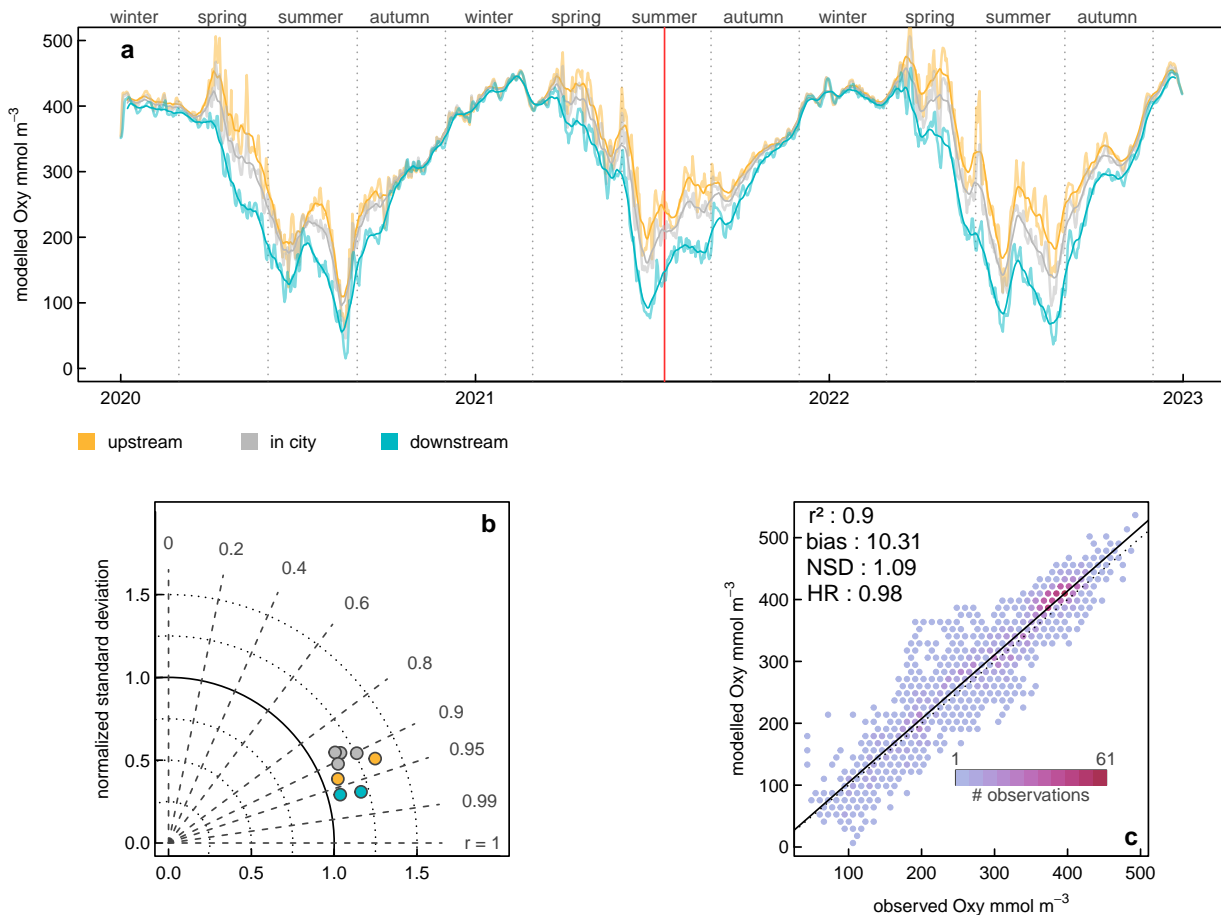


**Figure 5: Modelled dissolved oxygen concentration.** (a) Modelled oxygen upstream in city and downstream (daily mean and 15-day rolling mean in light and dark colors, respectively). (b) Taylor diagram showing the eight stations independently, and (c) comparison of modelled and observed oxygen values. For a complete picture of the oxygen validation, see Fig. 8.

stratification are closely connected to oxygen dynamics (Fan et al., 2025). However, this has led to misconceptions about the relative importance of biochemical processes to explain hypoxia and anoxia in the Elbe River.

#### 4.1. The role of temperature in oxygen dynamics

The role of temperature in explaining oxygen deficits has often been limited to its physical effects: first, by reducing oxygen solubility in warmer water (Weiss, 1970), and second, by increasing stratification that isolates deep water, preventing efficient re-aeration (Pein et al., 2021; Fan et al., 2025; van Vliet et al., 2023). Nevertheless, temperature-sensitivity in biochemical processes may have a stronger influence on the oxygen budget than previously accounted for. As water warms, oxygen-related processes become unbalanced due to differential temperature sensitivity in grazing (Verity et al., 2002; Ferreira et al., 2022), micro-algae growth rates (Sherman et al., 2016; Anderson et al., 2021), photosynthesis-light responses (Coles and Jones, 2000), viral infections (Padhy and Singh, 1977), and other chemical

rates (Garnier et al., 1999). Our model-based analysis emphasizes that the differential sensitivity of biochemical rates to temperature changes is a key factor driving seasonal variations in (de)oxygenation. As temperature fluctuates throughout the year, the rates of photosynthesis, respiration, mineralization, and nitrification respond differently, leading to shifts in overall ecosystem dynamics. These effects are not always accounted for in other model applications that assume the same sensitivities across all biochemical processes (e.g., Huang et al., 2017).

Our results suggest that the account for the differential temperature sensitivity in oxygen-related biochemical processes is key for evaluating the effects of climate warming (Hein et al., 2018) or transitory extreme events such as heatwaves in oxygen dynamics (van Vliet et al., 2023; Lyu et al., 2025). Most models implement a uniform temperature sensitivity—all processes are affected by temperature changes in the same magnitude, thus creating responses that vary in magnitude but not in the relative importance of each process (Huang et al., 2017). This may be problematic for

identifying the processes explaining oxygen dynamics. Also other processes found relevant in our study are usually absent in models: for example, pathogens—here viral infection, is systematically neglected in models with explicit oxygen dynamics (e.g., Yakushev et al., 2013; Neumann et al., 2022). Viral lysis is a potentially important mortality term for micro-algae (Wirtz, 2019; Elovaara et al., 2020; Krishna et al., 2024) and an important source of organic material that fuels high mineralization rates downstream.

#### 4.2. Changes in oxygen co-occur with other leading biochemical processes

In rivers, the oxygen dynamics shape other biochemical processes through positive or negative feedbacks (Carter et al., 2021; Lewis et al., 2024). For example, denitrification—the mineralization of organic material using the oxygen present in  $\text{NO}_3$ , which is subsequently reduced to  $\text{N}_2\text{O}$  and  $\text{N}_2$ —increases under low oxygen conditions and indirectly influences the oxygen budget in two ways (Zeng et al., 2019). First, denitrification can positively affect the oxygen budget due to its contribution to organic matter mineralization, thus decreasing oxygen consumption. Secondly, organic matter mineralization produces ammonia, which increases oxygen demand due to nitrification (Cai et al., 2022). In a river, this oxygen consumption may occur downstream, explaining the prominence of nitrification after the city (Fig. 3a).

The potent greenhouse gas  $\text{N}_2\text{O}$  is an intermediate product during both denitrification and nitrification (Bräse et al., 2017), with nitrification being the dominant source in the Elbe River. Its production and destruction are tightly linked to oxygen dynamics: lower oxygen is associated with higher  $\text{N}_2\text{O}$ , while under anoxic conditions  $\text{N}_2\text{O}$  is further reduced by denitrification (Stenström et al., 2014). The amount of nitrous oxide produced during nitrification and denitrification can vary widely, making it difficult to estimate its emissions from rivers. Estimates or measurements of  $\text{N}_2\text{O}$  yields range from 0.01 to 1%; Beaulieu et al. (2011) found a median value of less than 1% across 72 streams in the United States; de Wilde and de Bie (2000) found factors between 0.1 and 0.4% for nitrification in the Scheldt estuary. In the Elbe, Ingeniero et al. (2024) observed usually less than 0.1% of dissolved inorganic nitrogen in the form of  $\text{N}_2\text{O}$ , but elevated levels (up to  $40 \text{ nmol L}^{-1}$ ) were found in the Hamburg port area. Bräse et al. (2017) had previously observed up to  $52 \text{ nmol L}^{-1}$  in this area. While the river is usually saturated with  $\text{N}_2\text{O}$ , it is oversaturated in summer up to 200% and therefore a source of  $\text{N}_2\text{O}$  to the atmosphere with emissions on the order of  $20 \mu\text{mol m}^{-2} \text{ d}^{-1}$  (Schulz et al., 2023). Intermittently and spatially restricted to the city area, supersaturation has been observed up to 400% (Bräse et al., 2017), with emissions around  $100 \mu\text{mol m}^{-2} \text{ d}^{-1}$  (Schulz et al., 2023). Preußler (2025) was able to represent this value in a preliminary modeling study using OxyPOM.

Similar dynamics to those of (de-)nitrification may occur with other processes whose effects on oxygen dynamics are unclear—or at least not trivial. For example, while viral lysis

can be viewed just as an additional mortality term for micro-algae, diseases may have complex feedback interactions with nutrient availability (Krishna et al., 2024; Thongthaisong et al., 2025), further impacting oxygen dynamics through increased photosynthesis rates. This process might be particularly important under low discharge and high irradiance conditions, where upstream water is nutrient-depleted (Kamjunke et al., 2021; Schulz et al., 2023), and photosynthesis may rely on local nutrient recycling. However, these positive effects are limited, as viral lysis increases labile POM, which rapidly consumes oxygen during mineralization and decreases light availability due to shading. Furthermore, local nutrient recycling is conditioned on high light availability, which partly explains low phytoplankton growth rate downstream of the city, where changes in channel depth and smaller flow velocities lead to POM accumulation and low light availability (Kerner, 2007).

#### 4.3. Missing bits may (not) matter

Our physical-biogeochemical model neglects a series of biological, chemical and physical processes linking oxygen and biochemical dynamics. Alike almost all biogeochemical models, OxyPOM ignores higher trophic levels, such as zooplankton, fish and marine mammals, which not only determine river ecology (van Neer et al., 2023; Biederick et al., 2025), but may cascade down to lower trophic levels and biogeochemistry (Pace et al., 1999; Eger and Baum, 2020). In OxyPOM, more complex predator dynamics is only expressed as a temperature-dependent mortality rate so that the model may miss relevant biological processes directly affecting dissolved oxygen. For example, when fish die due to low oxygen, the grazing pressure on the predators of micro-algae may be reduced, creating a sudden high predation pressure on micro-algae (Rettig and Smith, 2021) and, in consequence, reducing photosynthetic oxygen production. This together with increased organic matter degradation due to decreasing fish likely spurs a positive feedback loop. Therefore, the influence of trophic cascades during massive fish mortalities may define an important research gap also relevant for water quality and fisheries management.

Our model prescribes micro-algae with a fixed stoichiometry following the view that rivers are not nutrient limited and, due to a high turbidity, light is the limiting resource, as observed in the Elbe River (Rewrie et al., 2025). This reasonable simplification, however, may not be always valid, as water upstream can occasionally become nutrient-depleted (Kamjunke et al., 2021), especially in the future due to de-eutrophication efforts and changes in the river discharge (Schulz et al., 2023).

Although mineralization and nitrification are effectively the main biochemical pathways to oxygen consumption, other chemical reactions, such as  $\text{SO}_4$  formation, can be also significant (Spieckermann et al., 2022) in our study area. These reactions, together with others redox processes—Fe and Mn oxidation—are necessary to explain oxygen dynamics in hypoxic and anoxic waters and have been already

considered in other models (Yakushev et al., 2017). Especially, the continuous oxygen demand by the sediments is not explicitly resolved here. Such a missing oxygen sink may also be responsible for the the slight overestimation of oxygen levels in the simulations .

Finally, overlooked physical feedbacks may also impact (de)oxygenation, as for example in the role of suspended particulate matter for light availability. Suspended particulate matter is abundant in the city section of the river (Kerner, 2007), with the potential of changing light availability and enhancing vertical transport of POM in tidal affected environment (Li and Wirtz, 2025). This process, while critical to understand light limitation is overly simplified in our model. We assumed a constant concentration of inorganic suspended particulate matter through the year, while particle density depends on discharge (Baborowski et al., 2012), season (Tobias-Hünefeldt et al., 2024), and erosion intensity (after events) (Uber et al., 2022).

Additional shortcomings may originate from the physical limitations of a simplified topology. For example, our simple one-channel funnel-like setup ignores much of the complexity on the water channels in the city. More realistic and numerically demanding modelling applications, find that these features can become critical for oxygen dynamics and phytoplankton persistence (Fan et al., 2025; Steidle and Vennell, 2024).

Despite all these limitations, our model configuration achieves high levels of accuracy comparable with other studies (Holzwarth and Wirtz, 2018; Pein et al., 2021; Fan et al., 2025) or even better (Schroeder, 1997; Schöl et al., 2014; Hein et al., 2018). A two-dimensional vertically resolved long-channel topology describes the oxygen related processes in the peri-urban area roughly in par with a three-dimensional set-up; adding a vertical dimension to a prior one-dimensional topology introduces important physicochemical feedbacks—e.g., stratification and re-aeration. Our model approach especially reproduces low oxygen levels, a difficult task for other models (Schöl et al., 2014; Hein et al., 2018). We could attribute this in part to (1) the differential temperature-dependencies of the biochemical and ecological processes, and (2) a an improved representations of light limitation and re-aeration..

Despite all these simplifications, limitations and omissions in biological, chemical and physical processes, our model configuration achieves high levels of accuracy comparable with other studies (Pein et al., 2021; Fan et al., 2025; Holzwarth and Wirtz, 2018) or even better (Schöl et al., 2014; Hein et al., 2018; Schroeder, 1997). A two-dimensional vertically resolved long-channel topology's performance for describing the oxygen processes in the peri-urban area is on par with a three-dimensional one; adding a vertical dimension to a prior one-dimensional topology introduces important physicochemical feedbacks—e.g., stratification and re-aeration. OxyPOM especially excels in reproducing low oxygen levels, a difficult task for other models (Schöl et al., 2014; Hein et al., 2018). We attribute

this to first, including the relevant processes the temperature-dependent nature of the biochemical process, and second, a vertical dimension with improved representations for light limitation and re-aeration, as well as of other sources of oxygen.

**Data availability.** All data was obtained from DWD <https://opendata.dwd.de> and used under CC BY 4.0 license(<https://www.dwd.de/copyright>); WSV (<https://www.kuestendaten.de>) and used under DL-DE->Zero-2.0 license (<https://www.govdata.de/dl-de/zero-2-0>); and FGG Elbe <https://www.elbe-datenportal.de> used under the terms of their proprietary license. Scripts to download third-party data required to reproduce analyses are freely available at <https://github.com/ovgarol/elbe-oxygen> and archived in Zenodo (García-Oliva and Lemmen, 2025).

The results of our simulations will be available at <https://pangaea.de/>.

**Code availability.** The source code for OxyPOM, GETM, and the Hamburg 2D setup are available at <https://codebase.helmholtz.cloud/dam-elbextreme/oxypom>, at <https://sourceforge.net/p/getm/code/ci/iow/tree>, and <https://codebase.helmholtz.cloud/dam-elbextreme/getm-setup-elbe-2d>, respectively. The source code for OxyPOM is also archived in Zenodo (García-Oliva and Lemmen, 2025). Custom scripts were used for simulation studies and data analyses. All code to generate figures is publicly available. All code is publicly available at <https://github.com/ovgarol/elbe-oxygen> and archived in Zenodo (García-Oliva and Lemmen, 2025).

**Acknowledgments.** This study was made possible by grants No. 03F0954D and No. 03F0954F of the German Federal Ministry of Research, Technology and Space (BMFTR) as part of the DAM mission “mareXtreme”, project “ElbeXtreme”; it was supported by the Helmholtz Association with their Innovation Pool for the Research Field Earth and Environment AGRIO: Effect of anthropogenic modifications and climate change on greenhouse gas emissions along the river-ocean continuum and, and through the joint research program “Changing Earth - Sustaining our Future”. This work used resources of the Deutsches Klimarechenzentrum (DKRZ) granted by its Scientific Steering Committee under project ID “gg0877”.

**Competing Interests Statement.** We declare to have no competing interests.

## CRediT authorship contribution statement

**Ovidio García-Oliva:** Conceptualization, Methodology, Data curation, Formal and statistical analysis, Software, Writing-original draft, Writing-review, and editing. **Carsten Lemmen:** Funding acquisition, Conceptualization, Software, Writing-original draft, Writing-review, and editing. **Xiangyu Li:** Software, Writing-review, and editing. **Kai Wirtz:** Funding acquisition, Formal analysis, Writing-review, and editing.

## References

Amann, T., Weiss, A., Hartmann, J., 2014. Silica fluxes in the inner Elbe Estuary, Germany. *Biogeochemistry* 118, 389–412. doi:10.1007/s10533-013-9940-3.

Anderson, S.I., Barton, A.D., Clayton, S., Dutkiewicz, S., Rynearson, T.A., 2021. Marine phytoplankton functional types exhibit diverse responses to thermal change. *Nat. Commun.* 12, 1–9. doi:10.1038/s41467-021-26651-8.

Ault, J.E., 2023. A River Runs through It: The Elbe, Socialist Security, and East Germany's Borders. *Cent. Eur. Hist.* 56, 196–213. doi:10.1017/S0008938922001030.

Baborowski, M., Simeonov, V., Einax, J.W., 2012. Assessment of Water Quality in the Elbe River at Flood Water Conditions Based on Cluster Analysis, Principle Components Analysis, and Source Apportionment. *Clean - Soil, Air, Water* 40, 373–380. doi:10.1002/clen.201100085.

Bastviken, D., Tranvik, L.J., Downing, J.A., Crill, P.M., Enrich-Prast, A., 2011. Freshwater methane emissions offset the continental carbon sink. *Science* 331, 50. doi:10.1126/science.1196808.

Beaulieu, J.J., et al., 2011. Nitrous oxide emission from denitrification in stream and river networks. *Proceedings of the National Academy of Sciences* 108, 214–219. doi:10.1073/pnas.1011464108.

Bernal, S., Ledesma, J.L.J., Peñarroya, X., Jativa, C., Catalán, N., Casamayor, E.O., Lupon, A., Marcé, R., Martí, E., Triadó-Margarit, X., Rocher-Ros, G., 2025. Expanding towards contraction: the alternation of floods and droughts as a fundamental component in river ecology. *Biogeochemistry* 168, 11. doi:10.1007/s10533-024-01197-1.

Biederick, J., Möllmann, C., Hauten, E., Russnak, V., Lahajnar, N., Hansen, T., Dierking, J., Koppelman, R., 2025. Spatial and temporal patterns of zooplankton trophic interactions and carbon sources in the eutrophic Elbe estuary (Germany). *ICES J. Mar. Sci.* 82. doi:10.1093/icesjms/fsae189.

Blaszcak, J.R., Koenig, L.E., Mejia, F.H., Gómez-Gener, L., Dutton, C.L., Carter, A.M., Grimm, N.B., Harvey, J.W., Helton, A.M., Cohen, M.J., 2023. Extent, patterns, and drivers of hypoxia in the world's streams and rivers. *Limnol. Oceanogr. Lett.* 8, 453–463. doi:10.1002/lo12.10297.

Branoff, B.B., Grüterich, L., Wilson, M., Tobias-Hunefeldt, S.P., Saadaoui, Y., Mittmann-Goetsch, J., Neiske, F., Lexmond, F., Becker, J.N., Grossart, H.P., Porada, P., Streit, W.R., Eschenbach, A., Kutzbach, L., Jensen, K., 2024. Partitioning biota along the Elbe River estuary: where are the community transitions?

Bräse, L., Bange, H.W., Lendt, R., Sanders, T., Dähnke, K., 2017. High resolution measurements of nitrous oxide (n<sub>2</sub>o) in the elbe estuary. *Frontiers in Marine Science* 4, 162. doi:10.3389/fmars.2017.00162.

Bruggeman, J., Bolding, K., 2014. A general framework for aquatic biogeochemical models. *Environ. Model. Softw.* 61, 249–265. doi:10.1016/j.envsoft.2014.04.002.

Burchard, H., Bolding, K., 2002. GETM – a general estuarine transport model. Scientific documentation. Tech. Rep. EUR 20253 en , 164.

Cai, M., Hong, Y., Wu, J., Moore, S.S., Vamerali, T., Ye, F., Wang, Y., 2022. Nitrate Addition Increases the Activity of Microbial Nitrogen Removal in Freshwater Sediment. *Microorganisms* 10. doi:10.3390/microorganisms10071429.

Carstens, M., Claussen, U., Bergemann, M., Gaumert, T., 2004. Transitional waters in Germany: The Elbe estuary as an example. *Aquat. Conserv. Mar. Freshw. Ecosyst.* 14, 81–92. doi:10.1002/aqc.652.

Carter, A.M., Blaszcak, J.R., Heffernan, J.B., Bernhardt, E.S., 2021. Hypoxia dynamics and spatial distribution in a low gradient river. *Limnol. Oceanogr.* 66, 2251–2265. doi:10.1002/lno.11751.

Casas-Ruiz, J.P., Catalán, N., Gómez-Gener, L., von Schiller, D., Obrador, B., Kothawala, D.N., López, P., Sabater, S., Marcé, R., 2017. A tale of pipes and reactors: Controls on the in-stream dynamics of dissolved organic matter in rivers. *Limnol. Oceanogr.* 62, S85–S94. doi:10.1002/lno.10471.

Coles, J.F., Jones, R.C., 2000. Effect of temperature on photosynthesis-light response and growth of four phytoplankton species isolated from a tidal freshwater river. *J. Phycol.* 36, 7–16. doi:10.1046/j.1529-8817.2000.98219.x.

Eger, A.M., Baum, J.K., 2020. Trophic cascades and connectivity in coastal benthic marine ecosystems: a meta-analysis of experimental and observational research. *Marine Ecology Progress Series* 656, 139–152.

Elovaara, S., Degerlund, M., Franklin, D.J., Kaartokallio, H., Tamelander, T., 2020. Seasonal variation in estuarine phytoplankton viability and its relationship with carbon dynamics in the Baltic Sea. *Hydrobiologia* 847, 2485–2501. doi:10.1007/s10750-020-04267-1.

European Commission, 2006. Indicators and methods for the ecological status assessment under the Water Framework Directive. Technical Report. Directorate-General Joint Research Centre Institute for Environment and Sustainability Luxembourg.

Fan, H., Pein, J., Chen, W., Staneva, J., Cheng, H., 2025. Effects of heatwave events on dissolved oxygen in the Elbe Estuary. *Water Res.* 286, 124125. doi:10.1016/j.watres.2025.124125.

Ferreira, G.D., Grigoropoulou, A., Saiz, E., Calbet, A., 2022. The effect of short-term temperature exposure on vital physiological processes of mixoplankton and protozooplankton. *Mar. Environ. Res.* 179, 105693. doi:10.1016/j.marenres.2022.105693.

García-Oliva, O., Lemmen, C., 2025. FABM OxyPOM and DiaMO: simple models for dissolved oxygen and biogeochemistry. doi:10.5281/zenodo.15111434.

Garnier, J., Billen, G., Palfner, L., 1999. Understanding the oxygen budget and related ecological processes in the river Mosel: The RIVER-STRÄHLER approach. *Hydrobiologia* 410, 151–166. doi:10.1023/A:1003894200796.

Graham, D.J., Bierkens, M.F., van Vliet, M.T., 2024. Impacts of droughts and heatwaves on river water quality worldwide. *J. Hydrol.* 629, 130590. doi:10.1016/j.jhydrol.2023.130590.

Grzyb, T., Kulczyk, S., 2023. How do ephemeral factors shape recreation along the urban river? A social media perspective. *Landsc. Urban Plan.* 230, 104638. doi:10.1016/j.landurbplan.2022.104638.

He, H., Boehringer, T., Schäfer, B., Heppell, K., Beck, C., 2024. Analyzing spatio-temporal dynamics of dissolved oxygen for the River Thames using superstatistical methods and machine learning. *Sci. Rep.* 14, 1–17. doi:10.1038/s41598-024-72084-w.

Hein, B., Viergutz, C., Wyrwa, J., Kirchesch, V., Schöl, A., 2018. Impacts of climate change on the water quality of the Elbe Estuary (Germany). *J. Appl. Water Eng. Res.* 6, 28–39. doi:10.1080/23249676.2016.1209438.

Holzwarth, I., Wirtz, K., 2018. Anthropogenic impacts on estuarine oxygen dynamics: A model based evaluation. *Estuar. Coast. Shelf Sci.* 211, 45–61. doi:10.1016/j.ecss.2018.01.020.

Huang, J., Yin, H., Chapra, S., Zhou, Q., 2017. Modelling Dissolved Oxygen Depression in an Urban River in China. *Water* 9, 520. doi:10.3390/w9070520.

Ingénierio, R.C.O., Dähnke, K., Sanders, T., et al., 2024. Dissolved nitric oxide in the lower elbe estuary and the port of hamburg area. *Biogeosciences* 21, 3425–3448. doi:10.5194/bg-21-3425-2024.

Kamjunke, N., Rode, M., Baborowski, M., Kunz, J.V., Zehner, J., Borchardt, D., Weitere, M., 2021. High irradiation and low discharge promote the dominant role of phytoplankton in riverine nutrient dynamics. *Limnol. Oceanogr.* 66, 2648–2660. doi:10.1002/lno.11778.

Kerner, M., 2007. Effects of deepening the Elbe Estuary on sediment regime and water quality. *Estuar. Coast. Shelf Sci.* 75, 492–500. doi:10.1016/j.ecss.2007.05.033.

Koll, R., Theilen, J., Hauten, E., Woodhouse, J.N., Thiel, R., Möllmann, C., Fabrizius, A., 2024. Network-based integration of omics, physiological and environmental data in real-world Elbe estuarine Zander. *Sci. Total Environ.* 942. doi:10.1016/j.scitotenv.2024.173656.

Krause, S., Abbott, B.W., Baranov, V., Bernal, S., Blaen, P., Datry, T., Drummond, J., Fleckenstein, J.H., Velez, J.G., Hannah, D.M., Knapp, J.L.A., Kurz, M., Lewandowski, J., Martí, E., Mendoza-Lera, C., Milner, A., Packman, A., Pinay, G., Ward, A.S., Zarnetze, J.P., 2022. Organizational Principles of Hyporheic Exchange Flow and Biogeochemical Cycling in River Networks Across Scales. *Water Resour. Res.* 58. doi:10.1029/2021WR029771.

Krishna, S., Peterson, V., Listmann, L., Hinnens, J., 2024. Interactive effects of viral lysis and warming in a coastal ocean identified from an idealized ecosystem model. *Ecol. Modell.* 487, 110550. doi:10.1016/j.ecolmodel.

2023.110550.

Lespez, L., Germaine, M.a., Gob, F., Tales, E., Thommeret, N., de Milleville, L., Archaimbault, V., Letourneur, M., 2025. A new tool to characterise the socio-environmental dimensions of urban rivers: Urban river socio-environmental index. *Landsc. Urban Plan.* 261, 105388. doi:10.1016/j.landurbplan.2025.105388.

Lewis, A.S.L., Lau, M.P., Jane, S.F., Rose, K.C., Be'eri-Shlevin, Y., Burnet, S.H., Clayer, F., Feuchtmayr, H., Grossart, H., Howard, D.W., Mariash, H., Delgado Martin, J., North, R.L., Oleksy, I., Pilla, R.M., Smagula, A.P., Sommaruga, R., Steiner, S.E., Verburg, P., Wain, D., Weyhenmeyer, G.A., Carey, C.C., 2024. Anoxia begets anoxia: A positive feedback to the deoxygenation of temperate lakes. *Glob. Chang. Biol.* 30, 1–19. doi:10.1111/gcb.17046.

Li, E., Wirtz, K., 2025. Aggregation of Suspended Particles Limited by Preferential Settling. *J. Geophys. Res. Ocean.* 130. doi:10.1029/2025JC022471.

Lyu, J., Shi, Y., Liu, T., Xu, X., Liu, S., Yang, G., Peng, D., Qu, Y., Zhang, S., Chen, C., Zhang, Y., Gao, J., 2025. Extreme drought-heatwave events threaten the biodiversity and stability of aquatic plankton communities in the Yangtze River ecosystems. *Commun. Earth Environ.* 6, 1–12. doi:10.1038/s43247-025-02143-1.

Ma, R., Chen, Z., Wang, B., Xu, C., Jia, Z., Li, L., Hu, J., 2024. Spatiotemporal variations and controlling mechanism of low dissolved oxygen in a highly urbanized complex river system. *J. Hydrol. Reg. Stud.* 52, 101691. doi:10.1016/j.ejrh.2024.101691.

Mallin, M.A., Johnson, V.L., Ensign, S.H., MacPherson, T.A., 2006. Factors contributing to hypoxia in rivers, lakes, and streams. *Limnol. Oceanogr.* 51, 690–701. doi:10.4319/lo.2006.51.1\_part\_2.00690.

Martens, N., Biederbick, J., Schaum, C.E., 2024a. Picophytoplankton prevail year-round in the Elbe estuary. *Plant-Environment Interact.* 5, 1–11. doi:10.1002/peiz.3.70014.

Martens, N., Russnak, V., Woodhouse, J., Grossart, H.P., Schaum, C.E., 2024b. Metabarcoding reveals potentially mixotrophic flagellates and picophytoplankton as key groups of phytoplankton in the Elbe estuary. *Environ. Res.* 252, 119126. doi:10.1016/j.envres.2024.119126.

van Neer, A., Nachtsheim, D., Siebert, U., Taupp, T., 2023. Movements and spatial usage of harbour seals in the Elbe estuary in Germany. *Sci. Rep.* 13, 1–17. doi:10.1038/s41598-023-33594-1.

Neumann, T., Radtke, H., Cahill, B., Schmidt, M., Rehder, G., 2022. Non-Redfieldian carbon model for the Baltic Sea (ERGOM version 1.2) – implementation and budget estimates. *Geosci. Model Dev.* 15, 8473–8540. doi:10.5194/gmd-15-8473-2022.

Pace, M.L., Cole, J.J., Carpenter, S.R., Kitchell, J.F., 1999. Trophic cascades revealed in diverse ecosystems. *Trends in ecology & evolution* 14, 483–488.

Padhy, R.N., Singh, P.K., 1977. Effect of temperature on the adsorption and one-step growth of the Nostoc virus N-1. *Arch. Microbiol.* 115, 163–167. doi:10.1007/BF00406370.

Pein, J., Eisele, A., Sanders, T., Daewel, U., Stanev, E.V., van Beusekom, J.E., Staneva, J., Schrum, C., 2021. Seasonal Stratification and Biogeochemical Turnover in the Freshwater Reach of a Partially Mixed Dredged Estuary. *Front. Mar. Sci.* 8. doi:10.3389/fmars.2021.623714.

Pein, J., Staneva, J., Biederbick, J., Schrum, C., 2025. Model-based assessment of sustainable adaptation options for an industrialised meso-tidal estuary. *Ocean Model.* 194, 102467. doi:10.1016/j.ocemod.2024.102467.

Platt, T., Gallegos, C., Harrison, W., 1980. Photoinhibition of photosynthesis in natural assemblages of marine phytoplankton. *J. Mar. Res.* 38, 687–701.

Preußler, N., 2025. Nitrous oxide production and emission in the oxygen minimum zone of the Elbe estuary: A coupled hydrodynamic-biogeochemical model. Bachelor's thesis. Leuphana University Lüneburg, Lüneburg, Germany.

Raymond, P.A., Cole, J.J., 2001. Gas exchange in rivers and estuaries: Choosing a gas transfer velocity. *Estuaries* 24, 312–317. doi:10.2307/1352954.

Reese, L., Gräwe, U., Klingbeil, K., Li, X., Lorenz, M., Burchard, H., 2024. Local Mixing Determines Spatial Structure of Diahaline Exchange Flow in a Mesotidal Estuary: A Study of Extreme Runoff Conditions. *J. Phys. Oceanogr.* 54, 3–27. doi:10.1175/JPO-D-23-0052.1.

Rettig, J.E., Smith, G.R., 2021. Relative strength of top-down effects of an invasive fish and bottom-up effects of nutrient addition in a simple aquatic food web. *Environ. Sci. Pollut. Res.* 28, 5845–5853. doi:10.1007/s11356-020-10933-7.

Rewrie, L.C., Baschek, B., van Beusekom, J.E., Körtzinger, A., Petersen, W., Röttgers, R., Voynova, Y.G., 2025. Impact of primary production and net ecosystem metabolism on carbon and nutrient cycling at the land-sea interface. *Front. Mar. Sci.* 12, 1–21. doi:10.3389/fmars.2025.1548463.

Salk, K.R., Ostrom, P.H., Biddanda, B.A., Weinke, A.D., Kendall, S.T., Ostrom, N.E., 2016. Ecosystem metabolism and greenhouse gas production in a mesotrophic northern temperate lake experiencing seasonal hypoxia. *Biogeochemistry* 131, 303–319. doi:10.1007/s10533-016-0280-y.

Sanders, T., Schöl, A., Dähnke, K., 2018. Hot Spots of Nitrification in the Elbe Estuary and Their Impact on Nitrate Regeneration. *Estuaries and Coasts* 41, 128–138. doi:10.1007/s12237-017-0264-8.

Schaffrin, A., Niggemeier, J., Ranft, F., Bohne, M., Feinendegen, L., Sternberger, J., Bernhardt, T., Lechne, L., 2021. Analysis of public confidence in scientific results related to northern European estuaries. Technical Report. ifok GmbH. Düsseldorf.

Scharfe, M., Callies, U., Blöcker, G., Petersen, W., Schroeder, F., 2009. A simple Lagrangian model to simulate temporal variability of algae in the Elbe River. *Ecol. Model.* 220, 2173–2186. doi:10.1016/j.ecolmodel.2009.04.048.

Schöl, A., Hein, B., Wyrwa, J., Kirchesch, Volker, 2014. Modelling Water Quality in the Elbe and its Estuary Large Scale and Long Term Applications with Focus on the Oxygen Budget of the Estuary. *Kusten*, 203–232.

Schroeder, F., 1997. Water quality in the Elbe estuary: Significance of different processes for the oxygen deficit at Hamburg. *Environ. Model. Assess.* 2, 73–82. doi:10.1023/a:1019032504922.

Schulz, G., van Beusekom, J.E., Jacob, J., Bold, S., Schöl, A., Ankele, M., Sanders, T., Dähnke, K., 2023. Low discharge intensifies nitrogen retention in rivers – A case study in the Elbe River. *Sci. Total Environ.* 904. doi:10.1016/j.scitotenv.2023.166740.

Schwentner, M., Zahir, R., Yamamoto, S., Husemann, M., Kullmann, B., Thiel, R., 2021. eDNA as a tool for non-invasive monitoring of the fauna of a turbid, well-mixed system, the Elbe estuary in Germany. *PLoS One* 16, 1–16. doi:10.1371/journal.pone.0250452.

Sherman, E., Moore, J.K., Primeau, F., Tanouye, D., 2016. Temperature influence on phytoplankton community growth rates. *Global Biogeochem. Cycles* 30, 550–559. doi:10.1002/2015GB005272.

Spieckermann, M., Gröngröft, A., Karrasch, M., Neumann, A., Eschenbach, A., 2022. Oxygen Consumption of Resuspended Sediments of the Upper Elbe Estuary: Process Identification and Prognosis. *Aquat. Geochemistry* 28, 1–25. doi:10.1007/s10498-021-09401-6.

Steidle, L., Vennell, R., 2024. Phytoplankton retention mechanisms in estuaries: A case study of the Elbe estuary. *Nonlinear Process. Geophys.* 31, 151–164. doi:10.5194/npg-31-151-2024.

Stenström, F., Bakker, M., Brodén, V., Kvärnström, E., 2014. Oxygen-induced dynamics of nitrous oxide in water and off-gas during the treatment of digester supernatant. *Water Science and Technology* 69, 84–91. doi:10.2166/wst.2014.673.

Thongthaisong, P., Kasada, M., Grossart, H.P., Wollrab, S., 2025. Longer durability of host–parasite interaction increases host density. *Oikos* 2025, e11029. doi:10.1111/oik.11029.

Tobias-Hünefeldt, S.P., van Beusekom, J.E., Russnak, V., Dähnke, K., Streit, W.R., Grossart, H.P., 2024. Seasonality, rather than estuarine gradient or particle suspension/sinking dynamics, determines estuarine carbon distributions. *Sci. Total Environ.* 926, 171962. doi:10.1016/j.scitotenv.2024.171962.

Über, M., Rössler, O., Astor, B., Hoffmann, T., Van Oost, K., Hillebrand, G., 2022. Climate Change Impacts on Soil Erosion and Sediment Delivery to German Federal Waterways: A Case Study of the Elbe Basin. *Atmosphere (Basel)*, 13, 1–21. doi:10.3390/atmos13111752.

Verity, P.G., Wassmann, P., Frischer, M.E., Howard-Jones, M.H., Allen, A.E., 2002. Grazing of phytoplankton by microzooplankton in the

Barents Sea during early summer. *J. Mar. Syst.* 38, 109–123. doi:10.

1016/S0924-7963(02)00172-0.

van Vliet, M.T., Thorslund, J., Strokal, M., Hofstra, N., Flörke, M., Ehalt  
Macedo, H., Nkwasa, A., Tang, T., Kaushal, S.S., Kumar, R., van  
Griensven, A., Bouwman, L., Mosley, L.M., 2023. Global river water  
quality under climate change and hydroclimatic extremes. *Nat. Rev.  
Earth Environ.* 4, 687–702. doi:10.1038/s43017-023-00472-3.

Wanninkhof, R., 1992. Relationship between wind speed and gas exchange  
over the ocean. *J. Geophys. Res. Ocean.* 97, 7373–7382. doi:10.1029/  
92JC00188.

Wanninkhof, R., 2014. Relationship between wind speed and gas exchange  
over the ocean revisited. *Limnol. Oceanogr. Methods* 12, 351–362.  
doi:10.4319/lom.2014.12.351.

Weiss, R.F., 1970. The solubility of nitrogen, oxygen and argon in water  
and seawater. *Deep. Res. Oceanogr. Abstr.* 17, 721–735. doi:10.1016/  
0011-7471(70)90037-9.

de Wilde, H.P.J., de Bie, M.J.M., 2000. Nitrous oxide in the schelde estuary:  
production by nitrification and emission to the atmosphere. *Marine  
Chemistry* 69, 203–216. doi:10.1016/S0304-4203(99)00106-1.

Wilkinson, M.D., Dumontier, M., Aalbersberg, I.J., Appleton, G., Axton,  
M., Baak, A., Blomberg, N., Boiten, J.W., da Silva Santos, L.B., Bourne,  
P.E., et al., 2016. The fair guiding principles for scientific data manage-  
ment and stewardship. *Scientific data* 3, 1–9.

Wiltshire, K.H., Manly, B.F., 2004. The warming trend at Helgoland Roads,  
North Sea: Phytoplankton response. *Helgol. Mar. Res.* 58, 269–273.  
doi:10.1007/s10152-004-0196-0.

Wiltshire, K.H., Schroeder, F., 1994. Pigment patterns in suspended matter  
from the Elbe estuary, Northern Germany. *Netherlands J. Aquat. Ecol.*  
28, 255–265. doi:10.1007/BF02334193.

Wirtz, K.W., 2019. Physics or biology? Persistent chlorophyll accumulation  
in a shallow coastal sea explained by pathogens and carnivorous grazing.  
*PLoS One* 14. doi:10.1371/journal.pone.0212143.

Wirtz, K.W., Eckhardt, B., 1996. Effective variables in ecosystem models  
with an application to phytoplankton succession. *Ecol. Modell.* 92, 33–  
53. doi:10.1016/0304-3800(95)00196-4.

Yakushev, E.V., Debolskaya, E.I., Kuznetsov, I.S., Staalstrøm, A., 2013.  
Modelling of the meromictic fjord hunnibunn (Norway) with an oxygen  
depletion model (OxyDep). *Handb. Environ. Chem.* 22, 235–251.  
doi:10.1007/698{\textunderscore}2011{\textunderscore}110.

Yakushev, E.V., Protsenko, E.A., Bruggeman, J., Wallhead, P., Pakhomova,  
S.V., Yakubov, S.K., Bellerby, R.G., Couture, R.M., 2017. Bottom  
RedOx Model (BROM v.1.1): A coupled benthic-pelagic model for  
simulation of water and sediment biogeochemistry. *Geosci. Model Dev.*  
10, 453–482. doi:10.5194/gmd-10-453-2017.

Zeng, J., Chen, M., Guo, L., Lin, H., Mu, X., Fan, L., Zheng, M., Qiu,  
Y., 2019. Role of organic components in regulating denitrification in  
the coastal water of Daya Bay, southern China. *Environ. Sci. Process.  
Impacts* 21, 831–844. doi:10.1039/c8em00558c.

Zhi, W., Klingler, C., Liu, J., Li, L., 2023. Widespread deoxygenation  
in warming rivers. *Nat. Clim. Chang.* 13, 1105–1113. doi:10.1038/  
s41558-023-01793-3.

## A. Full model description

### A.1. Re-aeration and water-air oxygen exchange

Oxygen transport due to aeration is calculated using the phenomenological equations of Wanninkhof (1992, 2014). The oxygen surface flux is

$$\text{Re-aeration} = \alpha \cdot k_{\text{air}} \cdot (\text{Sat} - \text{Oxy}), \quad (\text{A.1})$$

where  $\alpha$  is a form factor that corrects surface to volume ratio of idealized topologies (Holzwarth and Wirtz, 2018), oxygen is the dissolved oxygen in water, and Sat is the saturation oxygen concentration in water as function of temperature and salinity after (Weiss, 1970).  $k_{\text{air}}$  is the coefficient of re-aeration, which we defined as a function by parts corrected in low wind speeds after (Raymond and Cole, 2001)

$$k_{\text{air}} = \left( \frac{\text{Sc}}{660} \right)^{-0.5} \cdot \begin{cases} 0.0283 \cdot w^3, & \text{if } w \geq 11 \text{ m s}^{-1} \\ 0.3120 \cdot w^2, & \text{if } 11 > w \geq 3 \text{ m s}^{-1} \\ 0.9836 \cdot e^{0.35 \cdot w}, & \text{if } w < 3 \text{ m s}^{-1} \end{cases} \quad (\text{A.2})$$

where Sc is the Schmidt number, which depends on temperature and salinity (Wanninkhof, 2014), and  $w$  is the wind velocity in  $\text{m s}^{-1}$ . This formulation is new to the model as the original implementation was a vertical-averaged description (Holzwarth and Wirtz, 2018) and here we redefined the process to be vertically explicit.

### A.2. Micro-algae

The two micro-algae classes (one with dependence on dissolved silicate, thus representing diatoms) have growth rates that depend on photosynthesis, which is limited by light availability, dissolved nitrogen and ortho-phosphate concentrations.

$$\frac{d\text{Alg}_i}{dt} = \text{Alg}_i \cdot (\rho_i - m_i - r_i - \lambda_i), \quad (\text{A.3})$$

where  $\rho_i$  is the gross production rate,  $m_i$  is loss rate (mortality),  $r_i$  is the respiration rate and  $\lambda_i$  is the virus related mortality for each micro-algae.

The gross primary production is defined as

$$\rho_i = f_{\text{light},i} \cdot f_{\text{nut},i} \cdot \tau_{\text{Alg},i}(T) \cdot \mu_i^*, \quad (\text{A.4})$$

where  $f_{\text{light},i}$  and  $f_{\text{nut},i}$  are growth limitation coefficients for nutrient and light,  $\mu_i^*$  is the maximum growth rate in optimal conditions—neither light nor nutrient limitation—at a reference temperature of  $T' = 20 \text{ }^{\circ}\text{C}$  and  $\tau_{\text{Alg},i}(T)$  is a temperature-sensitivity function defined as a  $Q_{10}$  rule

$$\tau_{\text{Alg},i}(T) = Q_{10,\text{Alg},i}^{\frac{T-T^*}{10}}. \quad (\text{A.5})$$

The limitation coefficients for light are defined as a saturating exponential

$$f_{\text{light},i} = 1 - e^{-I/I_i^*}, \quad (\text{A.6})$$

where  $I$  is the light intensity and  $I_i^*$  is a reference light intensity. The limitation coefficients for nutrients are defined as a Leibig's rule of the minimum

$$f_{\text{nut},i} = \min(f_{N,i}, f_{P,i}, f_{Si,i}), \quad (\text{A.7})$$

where each  $f_X$  follows a Monod equation with half saturations  $K_X$ , thus

$$f_{X,i} = \frac{X}{X + K_X}. \quad (\text{A.8})$$

As by convention  $\text{Alg}_1$  represents diatoms—silicate limited—and  $\text{Alg}_2$  other non-diatoms, we set  $f_{Si,2} = 1$  to avoid silica limitation in non-diatoms.

The mortality rate  $m_i$  is a piece-wise defined function defined after (Scharfe et al., 2009), which emulate temperature dependent grazing with inhibition during colder temperatures

$$m_i = m_i^* \cdot \begin{cases} \tau_m(T), & \text{for } T \geq 20^\circ\text{C} \\ 1, & \text{for } 5 < T < 20^\circ\text{C} \\ 0.33, & \text{for } T \leq 5^\circ\text{C.} \end{cases} \quad (\text{A.9})$$

The respiration rate  $r_i$  is divided in basal and maintenance respiration rates, weighted by a factor  $\pi$  as

$$r_i = \pi \cdot \rho + (1 - \pi) \cdot r_i^* \cdot \tau_{\text{Res}}(T), \quad (\text{A.10})$$

where  $r_i^*$  is the respiration rate at the reference temperature and  $\tau_{\text{Res}}$  is the temperature sensitivity. The virus related mortality or cell lysis  $\lambda_i$  depends on a step-function (Wirtz, 2019) defined as

$$\lambda_i = \frac{1}{1 + e^{S \cdot (1 - \text{Vir}_i)}}, \quad (\text{A.11})$$

where  $\text{Vir}_i$  is the extent of the viral infection, and  $S$  is a sensitivity of mortality to viral infection.

The oxygen produced by photosynthesis used in the oxygen budget Eq. 1 is the addition of the gross primary production of both micro-algae classes

$$\text{Photosynthesis} = \sum_{i \in (1,2)} \rho_i \cdot \text{Alg}_i, \quad (\text{A.12})$$

and the respiration rate is the sum of the respiration rates plus a rather small fraction  $c$  of the mortality rate to emulate grazers respiration

$$\text{Respiration} = \sum_{i \in (1,2)} (r_i + c \cdot m_i) \cdot \text{Alg}_i. \quad (\text{A.13})$$

### A.3. Nutrient uptake

Nutrient uptake follows a fixed stoichiometry approach where the cell composition remains constant. The uptake rate is thus proportional to the net primary production, i.e., gross primary production minus respiration. In the case of phosphorus and silica, which are represented as a single inorganic form, the uptake rates are straightforwardly calculated as

$$u_X = a_X \cdot \sum_{i \in (1,2)} (\rho_i - r_i) \cdot \text{Alg}_i, \quad (\text{A.14})$$

$a_X$  is the stoichiometric ratio of  $X$  relative to carbon.

For nitrogen, the ammonia uptake is preferred in a flexible way unless the ammonia concentration is too low when nitrate uptake are instead preferred. The fraction of ammonia uptake when ammonia concentration is below a critical value of 0.7 mmol m<sup>-3</sup> is

$$f_{\text{NH}_4} = \frac{\text{NH}_4}{\text{NH}_4 + \text{NO}_3}, \quad (\text{A.15})$$

Ammonia and nitrate uptake is thus defined as

$$u_{\text{NH}_4} = a_N \cdot f_{\text{NH}_4} \cdot \sum_{i \in (1,2)} (\rho_i - r_i) \cdot \text{Alg}_i, \quad (\text{A.16})$$

$$u_{\text{NO}_3} = a_N \cdot (1 - f_{\text{NH}_4}) \cdot \sum_{i \in (1,2)} (\rho_i - r_i) \cdot \text{Alg}_i. \quad (\text{A.17})$$

In the case of ammonia above the critical value, we assume that nitrate uptake is inhibited, thus setting  $f_{\text{NH}_4} = 1$ .

#### A.4. Particulate and dissolved organic matter

POM and DOM have an explicit elemental composition (carbon, nitrogen and phosphorus). POM is present in two qualities, which transition in the sequences labile  $\rightarrow$  semi-labile  $\rightarrow$  dissolved and labile  $\rightarrow$  dissolved. Labile and semi-labile POM follow the dynamics:

$$\frac{dPOX_L}{dt} = a_X \cdot (1 - f) \cdot (m_1 + m_2 + \lambda_1 + \lambda_2) - d_{X,L \rightarrow S} - d_{X,L \rightarrow D} - M_{X,L}, \quad (A.18)$$

$$\frac{dPOX_S}{dt} = d_{X,L \rightarrow S} - d_{C,S \rightarrow D} - M_{X,S}, \quad (A.19)$$

where  $X$  is either carbon, nitrogen or phosphorus, the subindexes  $L$ ,  $S$ , and  $D$  are for labile, semi-labile, and dissolved, respectively,  $f$  is the fraction of nutrient released by autolysis, the sum  $m_1 + m_2 + \lambda_1 + \lambda_2$  is the total loss rate including mortality and lysis rates for each micro-algae,  $d_{X,i \rightarrow j}$  are degradation rates from the quality  $i$  to the quality  $j$ , and  $M_{X,i}$  are mineralization rates.

POM and DOM mineralize to DOC, nitrogen and ortho-phosphate. Unlike for dissolved nutrients, dissolved carbon is calculated using a simple mass balance

$$\frac{dDOC}{dt} = d_{C,L \rightarrow D} + d_{C,S \rightarrow D} - M_{C,D}. \quad (A.20)$$

POM mineralization rates for the element  $X$  of quality  $i$  are defined as

$$M_{X,i} = k_{Min,i} \cdot \tau_{Min}(T) \cdot POX_i, \quad (A.21)$$

where  $k_{Min,i}$  are mineralization rate constants for the quality  $i$  and  $\tau_{Min}(T)$  is the temperature sensitivity.

Degradation rates are defined from the mineralization rates as

$$d_{X,i \rightarrow j} = \kappa_{i \rightarrow j} \cdot M_{X,i}, \quad (A.22)$$

where  $\kappa_{i \rightarrow j}$  is a factor for the decomposition from the quality  $i$  to the quality  $j$ .

#### A.5. Dissolved nitrogen, nitrification and mineral denitrification

Dissolved inorganic nitrogen is the sum of ammonium and nitrate and ammonium transitions to nitrate as a function of oxygen. The mass balance for dissolved inorganic nitrogen is thus

$$\frac{dNH_4}{dt} = a_N \cdot f \cdot (m_1 + m_2 + \lambda_1 + \lambda_2) + M_N - u_{NH_4} - \gamma, \quad (A.23)$$

$$\frac{dNO_3}{dt} = \gamma - M_{NO_3} - u_{NO_3}, \quad (A.24)$$

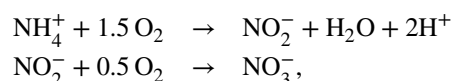
where  $\gamma$  is the ammonia consumed in the nitrification process,  $M_N$  is the total nitrogen mineralized from POM and DOM ( $= \sum_{i \in (L,S,D)} M_{N,i}$ ),  $M_{NO_3}$  is mineral denitrification into  $N_2$ ,  $u_{NH_4}$  and  $u_{NO_3}$  are total micro-algae uptake rates.

The ammonia used during nitrification depends on ammonia and oxygen concentrations as

$$\gamma = k_{Nit} \cdot \tau_{Nit}(T) \cdot \frac{NH_4}{NH_4 + K_{NH_4}} \cdot \frac{Oxy}{Oxy + K_{Oxy}^*}, \quad (A.25)$$

where  $K_{NH_4}$  and  $K_{Oxy}^*$  are half saturation constants for ammonia and oxygen in nitrification,  $k_{Nit}$  is the nitrification rate at the reference temperature and  $\tau_{Nit}(T)$  is the temperature sensitivity.

As the nitrification process consumes two moles of oxygen per each mol of nitrified ammonia in a two-step process



the total oxygen consumed during mineralization used in the oxygen budget (Eq. 1) is

$$\text{Nitrification} = 2 \cdot \gamma. \quad (\text{A.26})$$

Mineral denitrification is a fraction of total mineralized organics that is achieved by nitrate denitrification  $\Phi_N$  in contrast to oxygen consumption as a competing mechanism—which is proportional to  $(1 - \Phi_N)$ —thus

$$M_{\text{NO}_3} = \Phi_N \cdot \sum_{i \in (L, S, D)} M_{C,i} \text{ with } \Phi_N = \frac{\phi_N}{\phi_N + \phi_{\text{Oxy}}} \quad (\text{A.27})$$

where  $\phi_N$  and  $\phi_{\text{Oxy}}$  are contributions of nitrate and oxygen in mineralization defined as

$$\phi_N = \frac{\text{NO}_3}{\text{NO}_3 + K_{\text{NO}_3}} \cdot \left( 1 - \frac{\text{Oxy}}{\text{Oxy} + K_{\text{Oxy}}} \right) \cdot \tau_N(T) \quad (\text{A.28})$$

$$\phi_{\text{Oxy}} = \frac{\text{Oxy}}{\text{Oxy} + K'_{\text{Oxy}}} \cdot \tau_{\text{Oxy}}(T), \quad (\text{A.29})$$

where  $K_{\text{NO}_3}$ ,  $K_{\text{Oxy}}$  and  $K'_{\text{Oxy}}$  are half saturation constants for nitrate in denitrification, oxygen inhibition in denitrification and oxygen consumption in mineralization, and  $\tau_i$  are temperature-sensitivities with an appropriate  $Q_{10}$  value.

The oxygen consumed during mineralization used in the oxygen budget (Eq. 1) is

$$\text{Mineralization} = (1 - \Phi_N) \cdot \sum_{i \in (L, S, D)} M_{C,i}. \quad (\text{A.30})$$

## A.6. Ortho-phosphate and silicate

Ortho-phosphate is similar

$$\frac{d\text{PO}_4}{dt} = a_P \cdot f \cdot (m_1 + m_2 + \lambda_1 + \lambda_2) + M_P - u_{\text{PO}_4} \quad (\text{A.31})$$

where  $M_P$  is the total phosphorus mineralized from POM and DOM ( $= \sum_{i \in (L, S, D)} M_{P,i}$ ), and  $u_{\text{PO}_4}$  is the total micro-algae uptake rates for ortho-phosphate.

Unlike the other nitrogen and phosphorus, silicate is present in dissolved –bio-available– and particulate mineral (Opal) forms

$$\frac{dsi}{dt} = a_{\text{Si}} \cdot f \cdot (m_1 + \lambda_1) + D_{\text{Si}} - u_{\text{Si}}, \quad (\text{A.32})$$

$$\frac{d\text{Opal}}{dt} = a_{\text{Si}} \cdot (1 - f) \cdot m_1 - D_{\text{Si}} \quad (\text{A.33})$$

where  $D_{\text{Si}}$  is the dissolution rate of opal to bio-available dissolved silicate defined as

$$D_{\text{Si}} = k_{\text{Si}} \cdot \text{Opal} \cdot (\text{Si}' - \text{Si}), \quad (\text{A.34})$$

where  $k_{\text{Si}}$  is opal dissolution reaction rate constant, and  $\text{Si}'$  is a reference (saturation) bio-available silicate concentration. Note that the equations for silicate balance include only one micro-algae class, which represents diatoms.

## A.7. Viral infection

We consider two different virus, each one exclusively infecting either  $\text{Alg}_1$  or  $\text{Alg}_2$ . The dynamics in intracellular viral density  $\text{Vir}_i$  is here described by

$$\frac{d\text{Vir}_i}{dt} = G_i \cdot n_i - H_i - B_i, \quad (\text{A.35})$$

where  $G_i$  is infection–replication,  $n_i$  is the burst size (relative number of viral particles produced per host),  $H_i$  virus removal by host mortality (lysis), and  $B_i$  is virus inactivation.

The infection–replication is expressed as the probability of an infected host contacting a susceptible one. This is hindered by high concentrations immune and inert particles. Based on collision dynamics, we use

$$G_i = G^* \cdot \frac{\text{Vir}_i^2}{\text{POC}_L + \text{POC}_S + \text{Alg}_j}, \quad (\text{A.36})$$

where  $G^*$  is a reference infection rate. The burst size is a temperature-dependent step-function as

$$n_i = n^* \cdot \tau_n(T) \cdot \frac{1}{1 + e^{S \cdot (\text{Vir}_i^* - \text{Vir}_i)}}, \quad (\text{A.37})$$

where  $n^*$  is the reference burst size when  $\text{Vir}_i$  is large enough,  $\tau_n$  is the temperature sensitivity, and  $\text{Vir}_i^*$  is a half-saturation value.

Virus removal by host mortality is defined as the preferential loss of heavily infected hosts. This is expressed as an increased host mortality because infected phytoplankton frequently undergo apoptosis. This selective removal of infected individuals leads to a relative increase in the survival of healthy or less infected hosts or species, thereby reducing the average viral density. This is expressed using trait dynamics formulation (Wirtz and Eckhardt, 1996)

$$H_i = \text{Vir}_i \cdot (\text{Vir}_i^* - \text{Vir}_i) \cdot e^{-\frac{\text{Alg}_i}{C}} \cdot \frac{\text{Vir}_i}{\text{Vir}_i + \text{Vir}'} \cdot \lambda_i^2 \cdot S \cdot e^{S \cdot (1 - \text{Vir}_i)}, \quad (\text{A.38})$$

where  $\text{Vir}'$  is a reference low-value for virus abundance and  $C$  is a constant that modulates plankton diversity (Wirtz, 2019). The first two terms  $\text{Vir}_i \cdot (\text{Vir}_i^* - \text{Vir}_i)$  are diversity of the infection levels as calculated as in a binomial trait (Wirtz and Eckhardt, 1996), and the exponential term  $e^{-\frac{\text{Alg}_i}{C}}$  emulates the genetic diversity—coupled to virus susceptibility—reduction during blooming phases. The virus removal due to preferential loss thus depends on the diversity of the levels of infection host and of the host defense. The term  $\frac{\text{Vir}_i}{\text{Vir}_i + \text{Vir}'}$  maintains the levels of infection to viable levels (Wirtz, 2019). The remaining terms are the first partial derivative of  $\lambda_i$  in respect to  $\text{Vir}_i$ , standard method for trait dynamics  $\frac{\partial \lambda_i}{\partial \text{Vir}_i} = \lambda_i^2 \cdot S \cdot e^{S \cdot (1 - \text{Vir}_i)}$

Virus inactivation  $B_i$  is expressed by

$$B_i = B^* \cdot \tau_B(T) \cdot \frac{\text{Vir}_i^2}{\text{Vir}_i + \text{Vir}'}, \quad (\text{A.39})$$

where  $B^*$  is a reference inactivation value, and  $\tau_B$  is the temperature dependence.

## A.8. Light attenuation

Light attenuation follows an exponential decay with an exponential coefficient  $\zeta$  defined by

$$\zeta = \zeta_0 + \epsilon_{\text{POC}} \cdot (\text{POC}_L + \text{POC}_S) + \epsilon_{\text{Alg}} \cdot (\text{Alg}_1 + \text{Alg}_2) + \epsilon_{\text{ISPM}} \cdot \text{ISPM}, \quad (\text{A.40})$$

where  $\zeta_0$  is the background attenuation coefficient,  $\epsilon_{\text{POC}}$ ,  $\epsilon_{\text{Alg}}$  and  $\epsilon_{\text{ISPM}}$  are specific attenuation coefficients for POM, micro-algae, and a constant concentration of inorganic suspended particulate matter (ISPM), respectively.

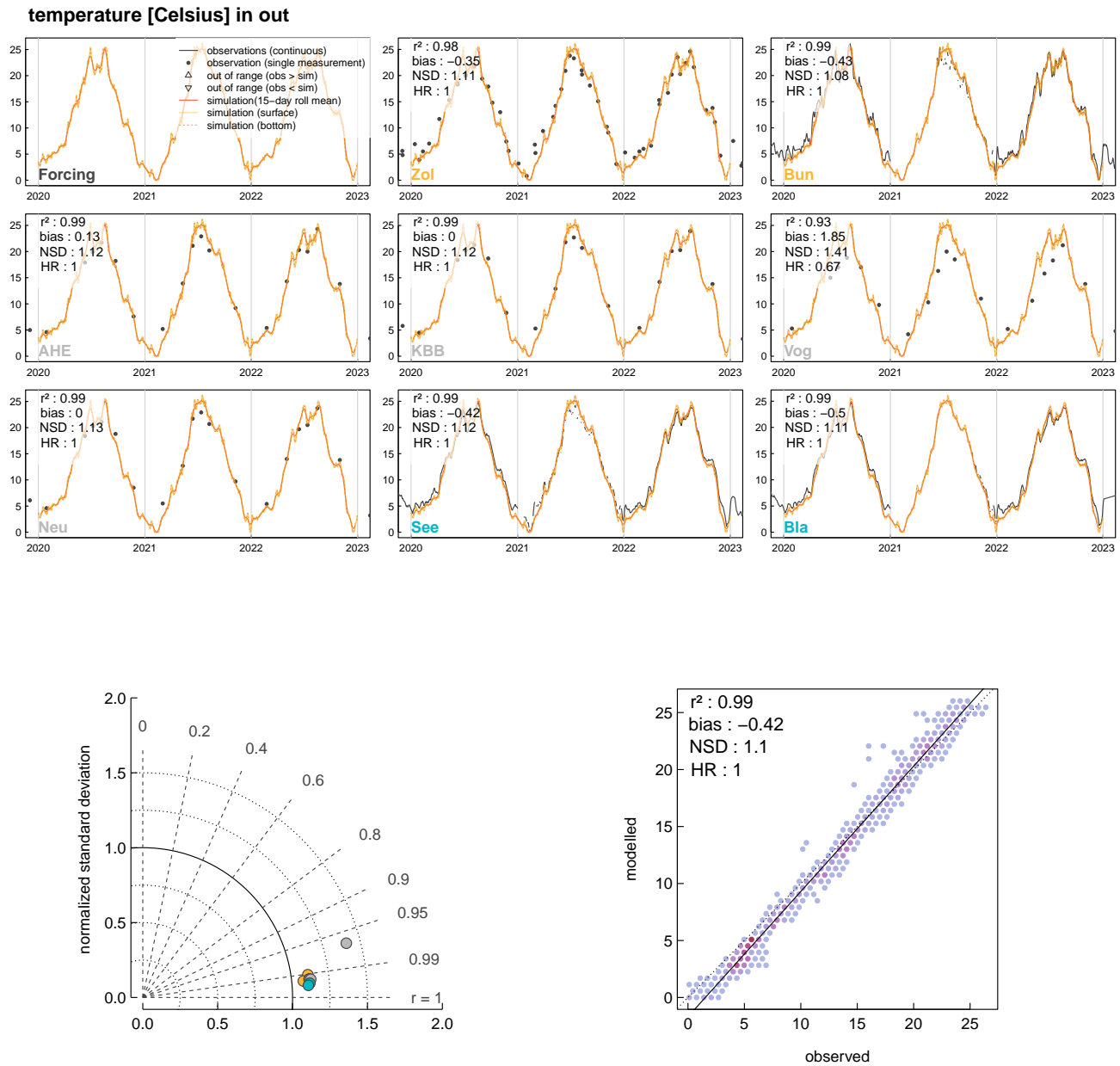
## A.9. Oxygen flux

The oxygen flux  $f$  is defined as the vertically integrated Oxy dynamics (Eq. 1) from the free surface ( $\eta = 0$ ) to the maximum depth  $\eta_{\text{max}}$  for each position along the river

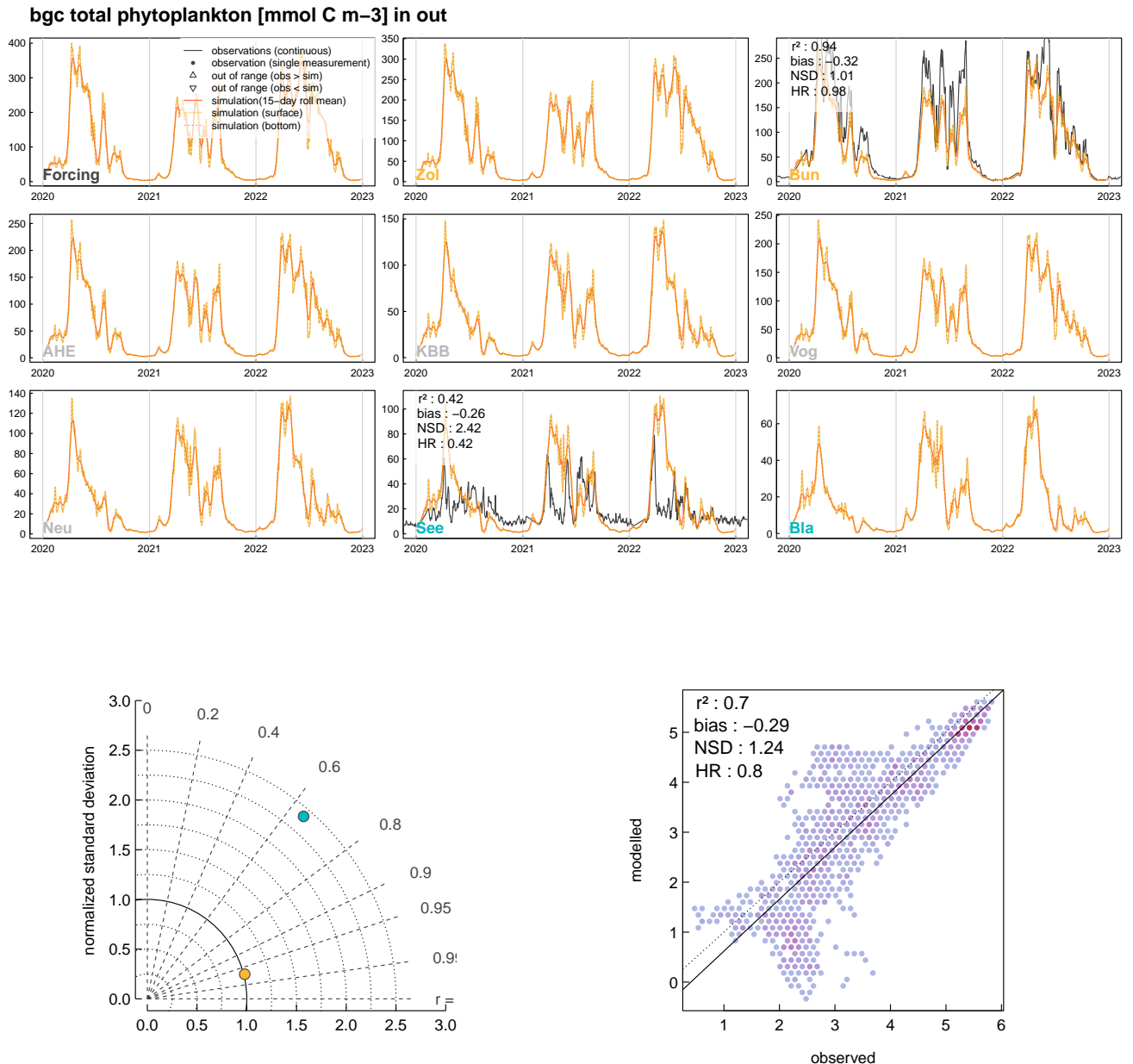
$$f = \int_{\eta=0}^{\eta_{\text{max}}} \frac{d\text{Oxy}}{dt} \cdot dz. \quad (\text{A.41})$$

## B. Extended model validation

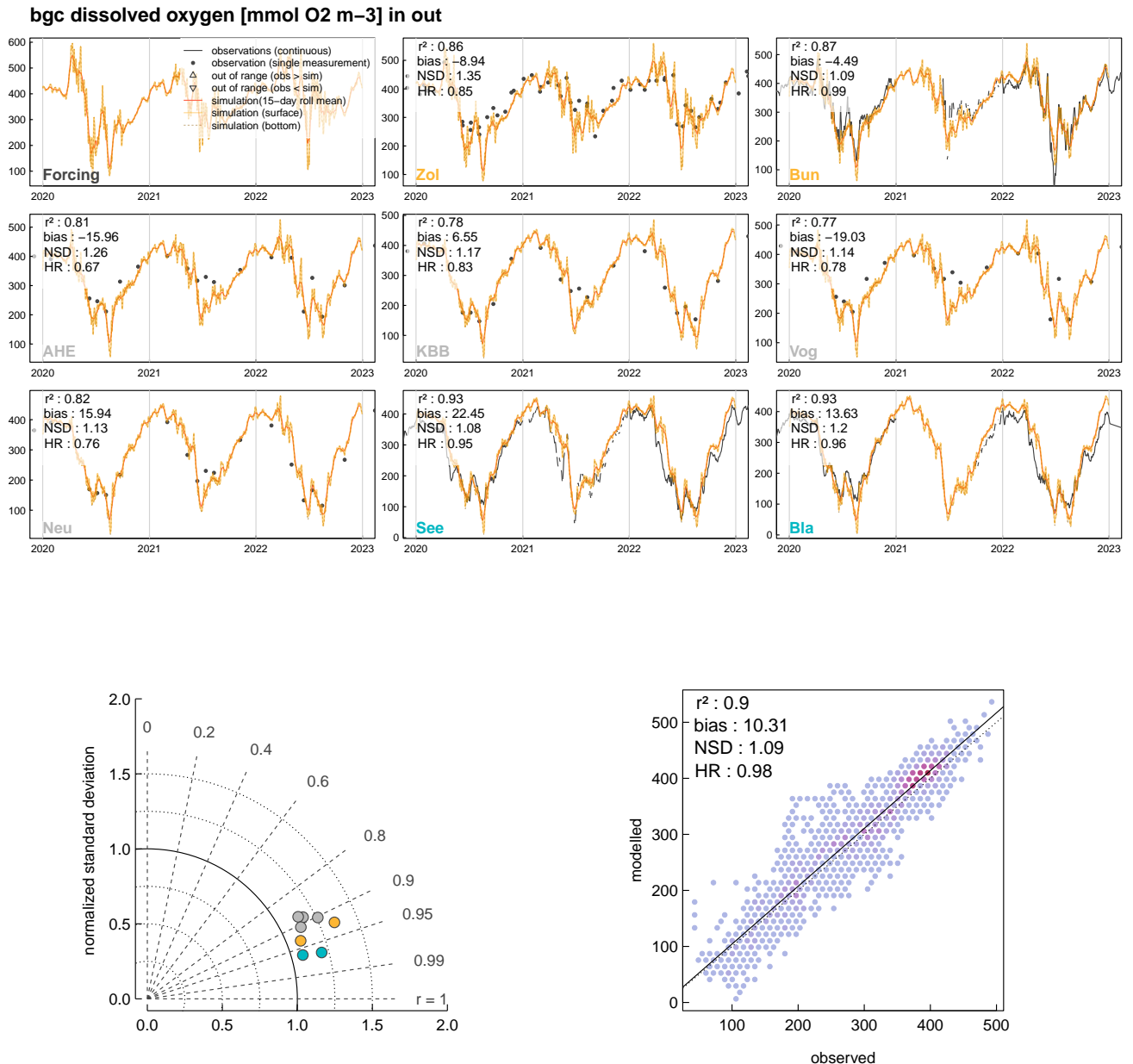
Our model application show high skill to reproduce observed values of temperature (Fig. 6), total micro-algae concentration (Fig. 7), dissolved oxygen (Fig. 8), nitrate (Fig. 9), ammonia (Fig. 10), ortho-phosphate (Fig. 11), and silica (Fig. 12).



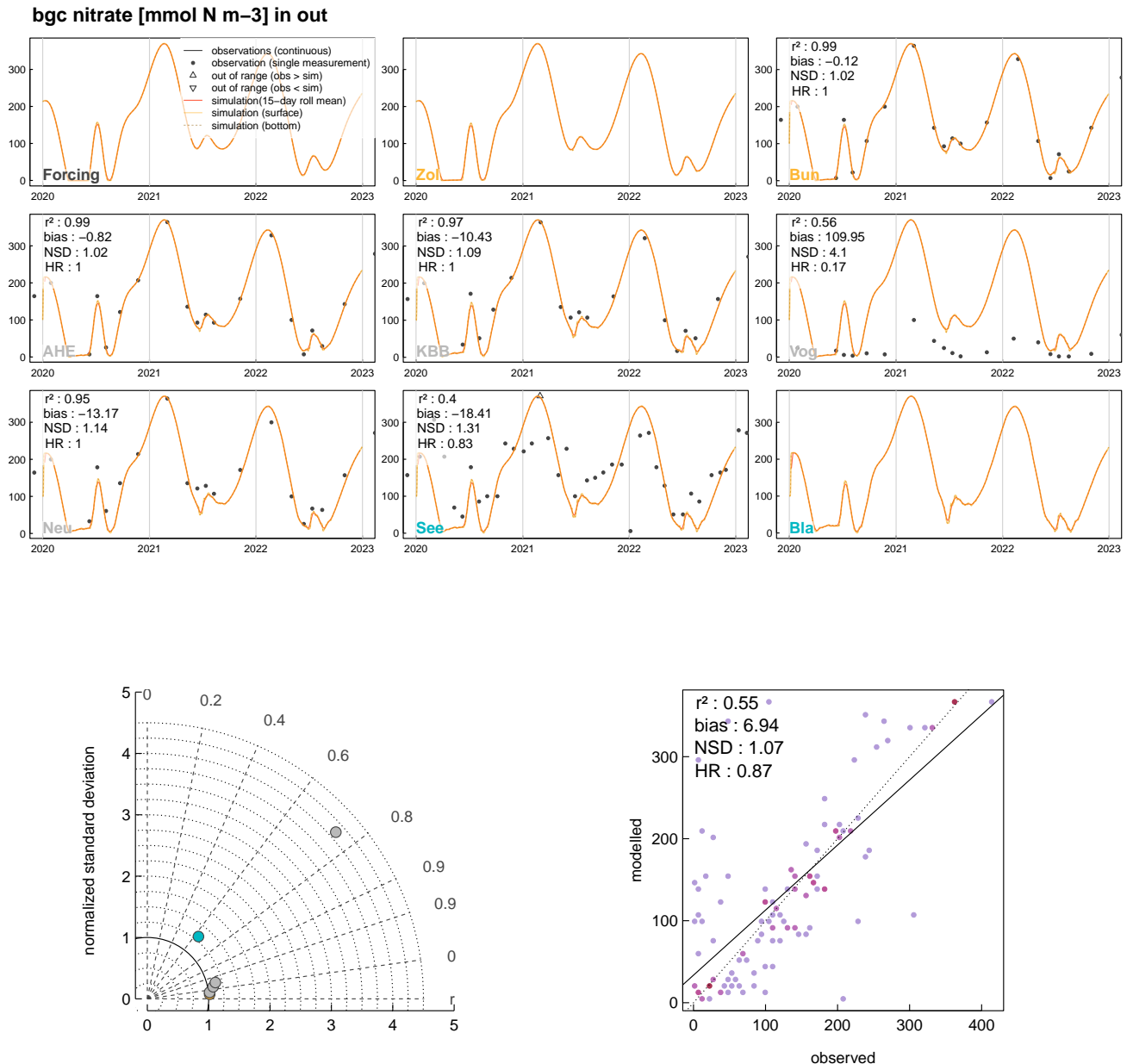
**Figure 6: Temperature validation:** Comparison of modelled (orange lines) and observed (black points and lines) values used as forcing in Geesthacht Wier and in each station (Zol = Zollenspieker, Bun = Bunthaus, AHE = Alte Harburger Elbbrücke, KBB = Köhlbrandbrücke, VNE = Vogelsander Norderelbe, Neu = Neumühlen, See = Seemannshöft, and Bla = Blankenese). In each plot, we included the performance metrics for each station ( $r^2$  = coefficient of determination, bias, NSD = normalized standard deviation, and HR = hit rate). The Taylor diagram (bottom left) and the aggregated observations vs. model comparison and their performance metrics (bottom right) are also shown.



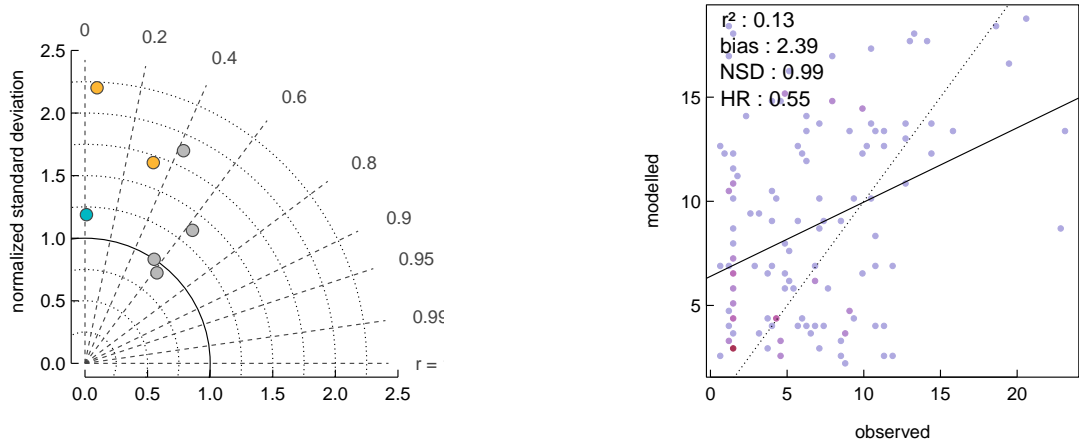
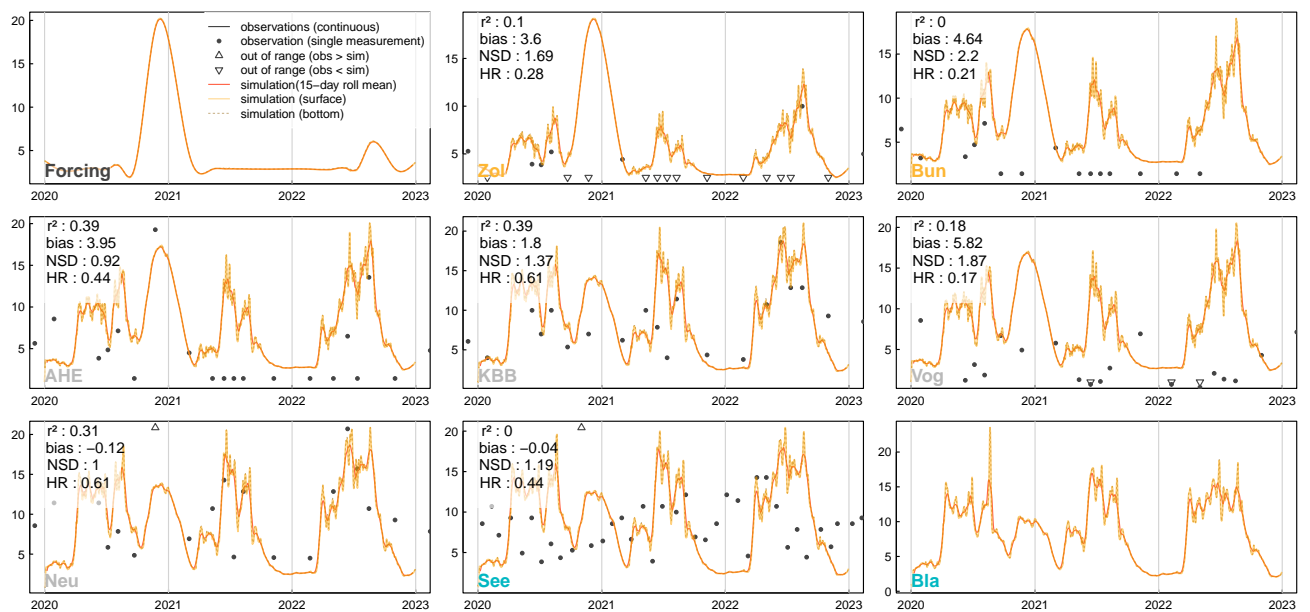
**Figure 7: Total phytoplankton (total sum of both micro-algae classes) validation:** Comparison of modelled (orange lines) and observed (black points and lines) values used as forcing in Geesthacht Wier and in each station (Zol = Zollenspieker, Bun = Bunthaus, AHE = Alte Harburger Elbbrücke, KBB = Köhlbrandbrücke, VNE = Vogelsander Norderelbe, Neu = Neumühlen, See = Seemannshöft, and Bla = Blankenese). In each plot, we included the performance metrics for each station ( $r^2$  = coefficient of determination, bias, NSD = normalized standard deviation, and HR = hit rate). The Taylor diagram (bottom left) and the aggregated observations vs. model comparisona and their performance metrics (bottom right) are also shown.



**Figure 8: Dissolved Oxygen validation:** Comparison of modelled (orange lines) and observed (black points and lines) values used as forcing in Geesthacht Wier and in each station (Zol = Zollenspieker, Bun = Bunthaus, AHE = Alte Harburger Elbbrücke, KBB = Köhlbrandbrücke, VNE = Vogelsander Norderelbe, Neu = Neumühlen, See = Seemannshöft, and Bla = Blankenese). In each plot, we included the performance metrics for each station ( $r^2$  = coefficient of determination, bias, NSD = normalized standard deviation, and HR = hit rate). The Taylor diagram (bottom left) and the aggregated observations vs. model comparison and their performance metrics (bottom right) are also shown.



**Figure 9: Nitrate validation:** Comparison of modelled (orange lines) and observed (black points and lines) values used as forcing in Geesthacht Wier and in each station (Zol = Zollenspieker, Bun = Bunthaus, AHE = Alte Harburger Elbbrücke, KBB = Köhlbrandbrücke, VNE = Vogelsander Norderelbe, Neu = Neumühlen, See = Seemannshöft, and Bla = Blankenese). In each plot, we included the performance metrics for each station ( $r^2$  = coefficient of determination, bias, NSD = normalized standard deviation, and HR = hit rate). The Taylor diagram (bottom left) and the aggregated observations vs. model comparison and their performance metrics (bottom right) are also shown.

bgc ammonia [mmol N m<sup>-3</sup>] in out

**Figure 10: Ammonia validation:** Comparison of modelled (orange lines) and observed (black points and lines) values used as forcing in Geesthacht Wier and in each station (Zol = Zollenspieker, Bun = Bunthaus, AHE = Alte Harburger Elbbrücke, KBB = Köhlbrandbrücke, VNE = Vogelsander Norderelbe, Neu = Neumühlen, See = Seemannshöft, and Bla = Blankenese). In each plot, we included the performance metrics for each station ( $r^2$  = coefficient of determination, bias, NSD = normalized standard deviation, and HR = hit rate). The Taylor diagram (bottom left) and the aggregated observations vs. model comparison and their performance metrics (bottom right) are also shown.

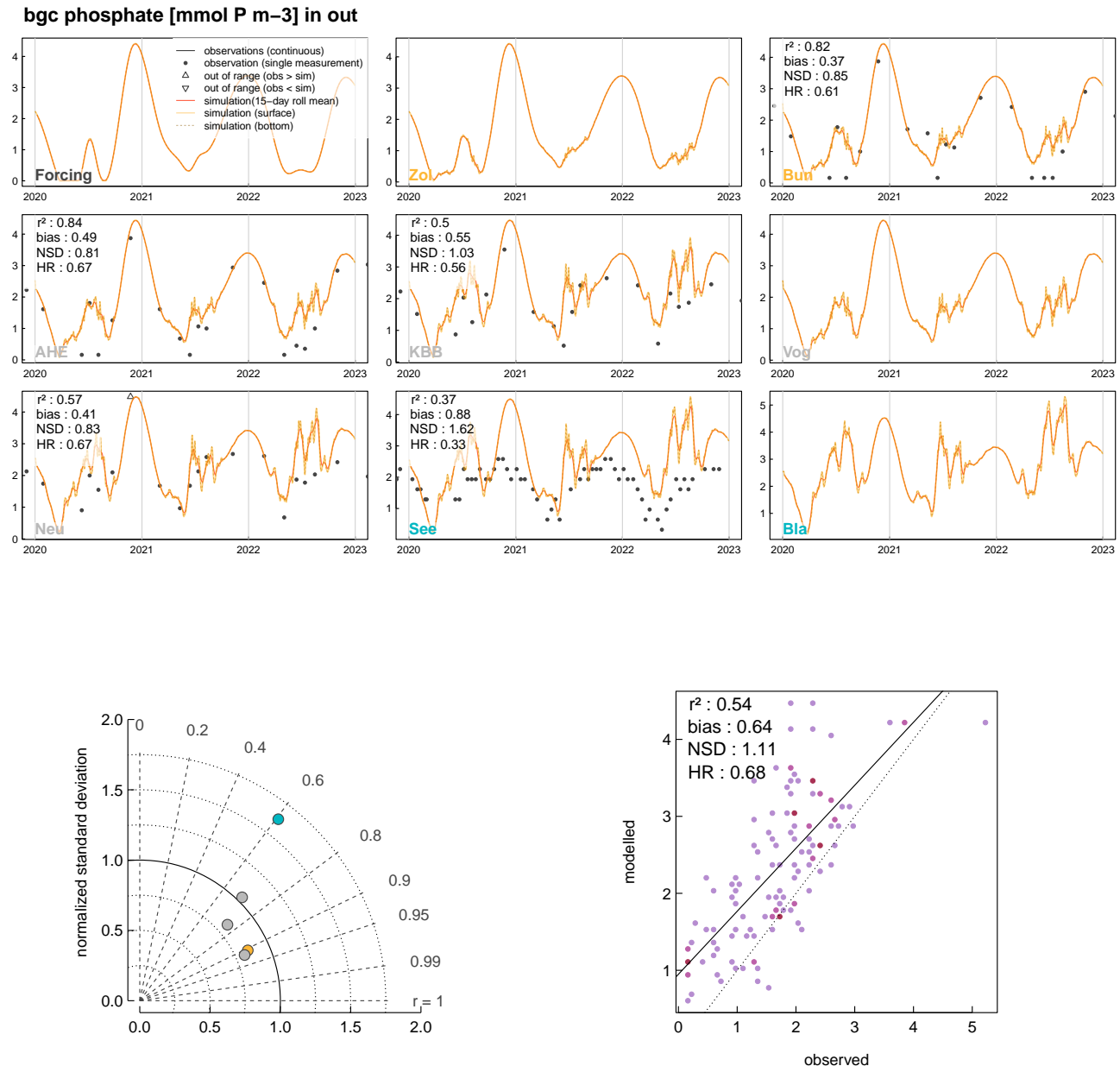


**Figure 11: Ortho-phosphate validation:** Comparison of modelled (orange lines) and observed (black points and lines) values used as forcing in Geesthacht Wier and in each station (Zol = Zollenspieker, Bun = Bunthaus, AHE = Alte Harburger Elbbrücke, KBB = Köhlbrandbrücke, VNE = Vogelsander Norderelbe, Neu = Neumühlen, See = Seemannshöft, and Bla = Blankenese). In each plot, we included the performance metrics for each station ( $r^2$  = coefficient of determination, bias, NSD = normalized standard deviation, and HR = hit rate). The Taylor diagram (bottom left) and the aggregated observations vs. model comparison and their performance metrics (bottom right) are also shown.

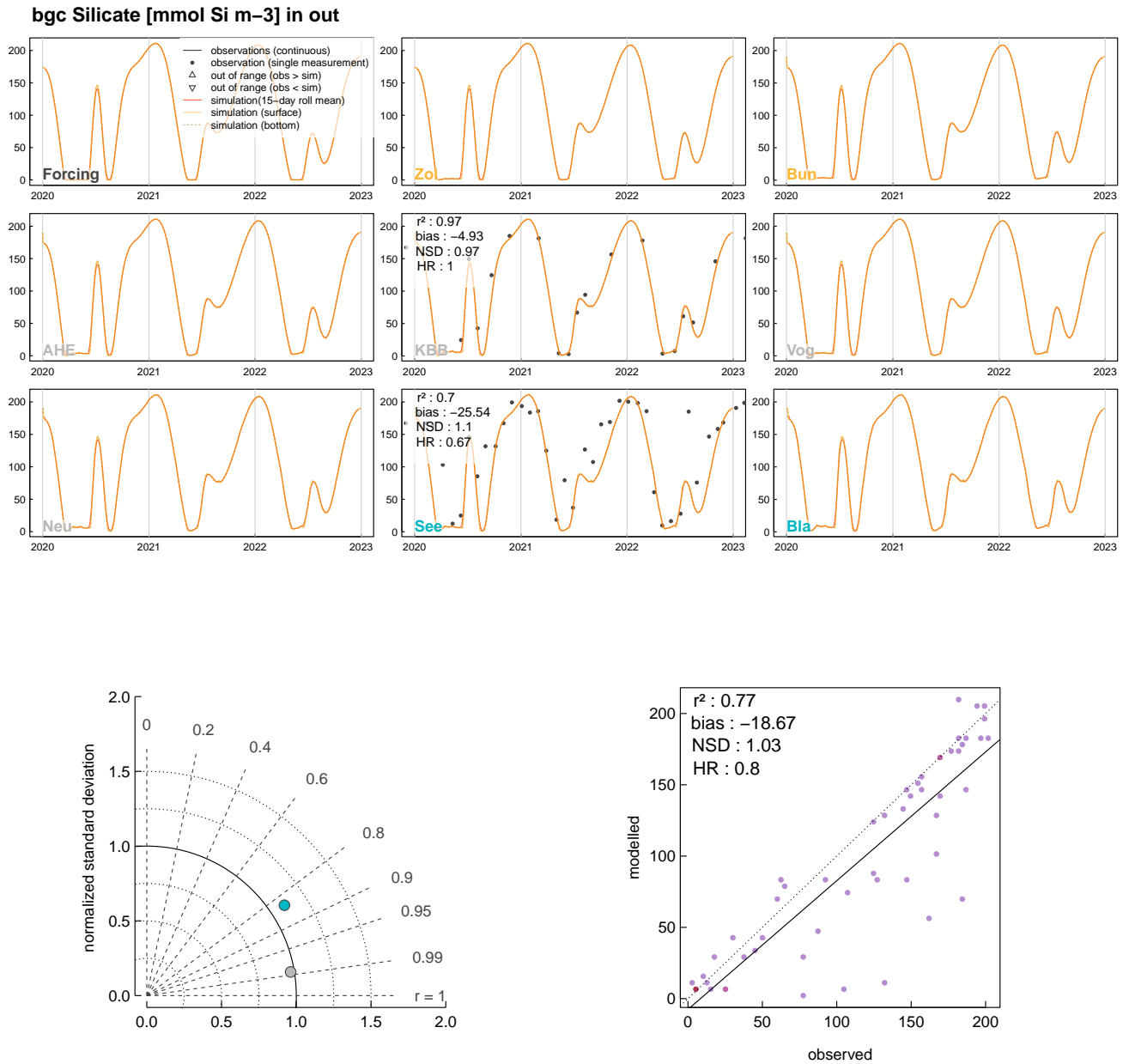


**Figure 12: Silica validation:** Comparison of modelled (orange lines) and observed (black points and lines) values used as forcing in Geesthacht Wier and in each station (Zol = Zollenspieker, Bun = Bunthaus, AHE = Alte Harburger Elbbrücke, KBB = Köhlbrandbrücke, VNE = Vogelsander Norderelbe, Neu = Neumühlen, See = Seemannshöft, and Bla = Blankenese). In each plot, we included the performance metrics for each station ( $r^2$  = coefficient of determination, bias, NSD = normalized standard deviation, and HR = hit rate). The Taylor diagram (bottom left) and the aggregated observations vs. model comparison and their performance metrics (bottom right) are also shown.